Large-Scale Whole-Exome Sequencing Association Study Implicates Genetic Effects on Viral Oncogenesis and Tumor Microenvironment in Nasopharyngeal Carcinoma

Yanni Zeng[1,2,3#], Chun-Ling Luo[1,4#], Guo-Wang Lin[5#], Fugui Li[6], Xiaomeng Bai[1,2,3], Josephine Mun-Yee Ko[7], Yang Liu[1,4], Shuai He[1,4], Jia-Xin Jiang[1,4], Wen-Xin Yan[1,4], Enya Hui Wen ONG[8], Zheng Li[9], Ya-Qing Zhou[1,4], Yun-He Zhou[1,4], An-Yi Xu[1,4], Shu-Qiang Liu[1,4], Yun-Miao Guo[10], Jie-Rong Chen[11], Xi-Xi Cheng[1,4], Yu-Lu Cao[1], Xia Yu[6], Biaohua Wu[6], Pan-Pan Wei[1,4], Zhao-Hui Ruan[1,4], Qiu-Yan Chen[1], Lin-Quan Tang[1], James D. McKay[12], Wei-Hua Jia[1], Hai-Qiang Mai[1], Jian-Jun Liu[13], Dong-Xin Lin[1], Chiea Chuen Khor[9], Melvin Lee Kiang CHUA[8,14,15*], Mingfang Ji[6*], Maria Li Lung[7*], Yi-Xin Zeng[1*], Jin-Xin Bei[1,4,16*†]

1. State Key Laboratory of Oncology in South China, Guangdong Key Laboratory of Nasopharyngeal Carcinoma Diagnosis and Therapy, Guangdong Provincial Clinical Research Center for Cancer, Sun Yat-sen University Cancer Center - Zhongshan School of Medicine, Sun Yat-sen University, Guangzhou, P.R. China
2. Faculty of Forensic Medicine, Guangdong Province Translational Forensic Medicine Engineering Technology Research Center, Zhongshan School of Medicine, Sun Yat-sen University, Guangzhou, P.R. China.
3. Guangdong Province Key Laboratory of Brain Function and Disease, Zhongshan School of Medicine, Sun Yat-sen University, Guangzhou, P.R. China.
4. Department of Experimental Research, Sun Yat-sen University Cancer Center, Guangzhou, P.R. China.
5. Department of Laboratory Medicine, Zhujiang Hospital, Southern Medical University, Guangzhou, Guangdong, P.R. China.
6. Cancer Research Institute of Zhongshan City, Zhongshan City People 's Hospital, Zhongshan, P.R. China.
7. Department of Clinical Oncology, School of Clinical Medicine, University of Hong Kong, Hong Kong SAR, P.R. China.
8. Precision Radiotherapeutics Oncology Programme, Division of Medical Sciences, National Cancer Centre Singapore, Singapore.
9. Genome Institute of Singapore (GIS), Agency for Science, Technology and Research (A*STAR), Singapore, Singapore.

10. Zhanjiang Institute of Clinical Medicine, Central People's Hospital of Zhanjiang, Guangdong Medical University Zhanjiang Central Hospital, Zhanjiang, P. R. China.
11. Department of Laboratory Medicine, Guangdong Provincial People's Hospital (Guangdong Academy of Medical Sciences), Southern Medical University, Guangzhou, P.R. China.
12. Genomic Epidemiology Branch, International Agency for Research on Cancer/World Health Organization (IARC/WHO), France.
13. Laboratory of Human Genomics, Genome Institute of Singapore, Agency for Science, Technology and Research (A*STAR), Singapore.
14. Department of Head and Neck and Thoracic Radiation Oncology, National Cancer Centre Singapore, Singapore.
15. Oncology Academic Clinical Programme, Duke-NUS Medical School, Singapore.
16. Department of Medical Oncology, National Cancer Centre Singapore, Singapore.

# These authors contributed equally.
* Senior authors who jointly directed the study.
† Correspondence to:
Dr Jin-Xin Bei, State Key Laboratory of Oncology in South China, Sun Yat-sen University Cancer Center, Guangzhou 510060, China
E-mail: beijx@sysucc.org.cn

Abstract

Nasopharyngeal carcinoma (NPC) poses a substantial clinical challenge with limited understanding of its genetic underpinnings. Here we conduct the largest-scale whole-exome sequencing association study of NPC to date, involving 6,969 NPC cases and 7,100 controls and revealing three novel germline genetic variants linked to NPC susceptibility: a common variant rs2276868 in *RPL14*, a rare variant rs5361 in *SELE*, and a common variant rs1050462 in *HLA-B*. Through a multiomics approach, which integrates both bulk (n=206) and single-cell RNA-sequencing (n=56) data along with experimental validations, we demonstrate that the *RPL14* variant modulates Epstein-Barr virus (EBV) life cycle and NPC pathogenesis. Additionally, we show that the *SELE* variant plays a role in modifying endothelial cell function, thus promoting NPC progression. Our study also underscores the critical impact of rare genetic variants on NPC heritability. We introduce a refined composite polygenic risk score (rcPRS) that outperforms existing models in predicting NPC risk. Notably, our findings reveal that the polygenic risk for NPC is mediated by EBV infection status. Overall, our study provides crucial insights into the intricate genetic architecture of NPC. It highlights the critical interplay between genetic variations and essential elements of the tumor microenvironment, such as EBV and endothelial cells, in predisposing to NPC. This work opens new avenues for personalized risk assessments, early diagnosis, and targeted therapeutic strategies for NPC.

Keywords

Nasopharyngeal carcinoma (NPC), whole-exome sequencing, genetic susceptibility, EBV, *RPL14, SELE,* HLA

95 **Introduction**

96 Nasopharyngeal carcinoma (NPC) is a highly lethal malignancy that exhibits a significant
97 geographic prevalence in specific regions of East and Southeast Asia[1]. These areas account for
98 approximately 70% of new cases worldwide[1], with the highest incidence rate (9.69/100,000)
99 reported in southern China area[2]. Familial clustering has been documented in a notable
100 proportion (3.64~19%) of NPC patients from diverse populations[3-6], suggesting a strong link
101 between family history and NPC risk[7]. Genetic susceptibility, Epstein-Barr virus (EBV)
102 infection, and environmental effects are believed to play essential roles in NPC development[1].

103 Efforts have been made to identify germline variations contributing to the genetic
104 susceptibility of NPC. Multiple linkage and association studies have reported that common
105 genetic variants in HLA region confer a significant risk for NPC[8-11]. Besides the HLA loci,
106 linkage studies have also identified risk loci in 4p12-p15, 3p21.31-21.2, and 5p13.1[9,12,13].
107 However, the replication of these linkage results has been challenging due to the diminishing
108 size of family pedigrees and the low resolution of reported loci, limiting their practical
109 application. Recently, genome-wide association studies (GWASs) have identified replicated
110 common single nucleotide polymorphism (SNPs) in multiple loci associated with NPC risk,
111 including *MECOM*, *CDKN2A/B*, *TNFRSF19*, *CIITA*, and *TERT/CLPTM1L*, in addition to the
112 HLA loci[8,14-17]. However, these GWAS loci explain only a small portion (2.84%) of the overall
113 NPC susceptibility[18], despite the relatively high heritability of NPC (10~61.3%)[19,20].

114 The issue of "missing heritability" (the gap between the heritability explained by GWAS
115 loci and the total heritability) in NPC, similar to other complex polygenic diseases, may be
116 attributed to the limited statistical power of studies targeting common variants (minor allele
117 frequency (MAF)>=0.01) and even poorer power of studies capturing rare variants
118 (MAF<0.01), such as those reported by utilizing whole-genome sequencing (WGS) or whole-
119 exome sequencing (WES) [21,22]. Currently, only a few studies have examined the contribution
120 of rare variants to NPC risk through WES, identifying NPC-associated genes such as *MST1R,*
121 *RAD54L* and *POLN* [23-26]. However, these findings either did not reach exome-wide statistical
122 significance or have not been independently validated, likely due to limited sample sizes or
123 genetic heterogeneity across population. Therefore, the genetic architecture involving both
124 common and rare variants in NPC risk remains unclear.

125 The role of EBV molecules in the screening and diagnosis of NPC is significant, as
126 evidenced by their presence in NPC tumor and peripheral blood[27,28]. This is particularly

127 remarkable given that over 90% of the adult population is infected with EBV[29]. However, the
128 exact mechanisms linking EBV to NPC, and the potential involvement of host genetic
129 variations in those processes, are still enigmatic. EBV is known for its ability to transform B
130 cells into lymphoblastoid cell lines and for encoding oncogenic genes such as LMP1 and
131 BARFs[30]. In NPC, EBV infects epithelial cells and encodes viral genes related to NPC
132 progression[31]. Furthermore, the interaction of EBV with malignant epithelial cells and various
133 stromal cell types, each exhibiting unique gene expression profiles, fosters a complex tumor
134 microenvironment (TME), leading to both intra- and inter-tumor heterogeneity in NPC[32,33].
135 Despite these insights, the influence of genetic variations on TME components, and how this
136 contributes to NPC predisposition remains elusive.

137 This study aims to deepen our understanding of the genetic architecture of NPC and to
138 translate genetic findings into insights about its pathological mechanisms. We first conducted
139 a comprehensive two-stage association study, utilizing WES and capture-sequencing (Cap-seq)
140 analyses across multiple levels—variant, gene, and pathway—involving 14,069 individuals of
141 southern Chinese descent, including those from Guangdong, Hong Kong in China, and
142 Singapore. Furthermore, we employed extensive bulk and single cell RNA sequencing analyses,
143 along with experimental assays, to elucidate the functional mechanisms of the identified risk
144 loci. Critically, we uncovered the profound impact of both common and rare genetic variants
145 on cancer heritability, particularly how these genetic variations distinctly affect EBV-related
146 pathogenesis and TME components, thereby contributing to varying susceptibilities to NPC.

147

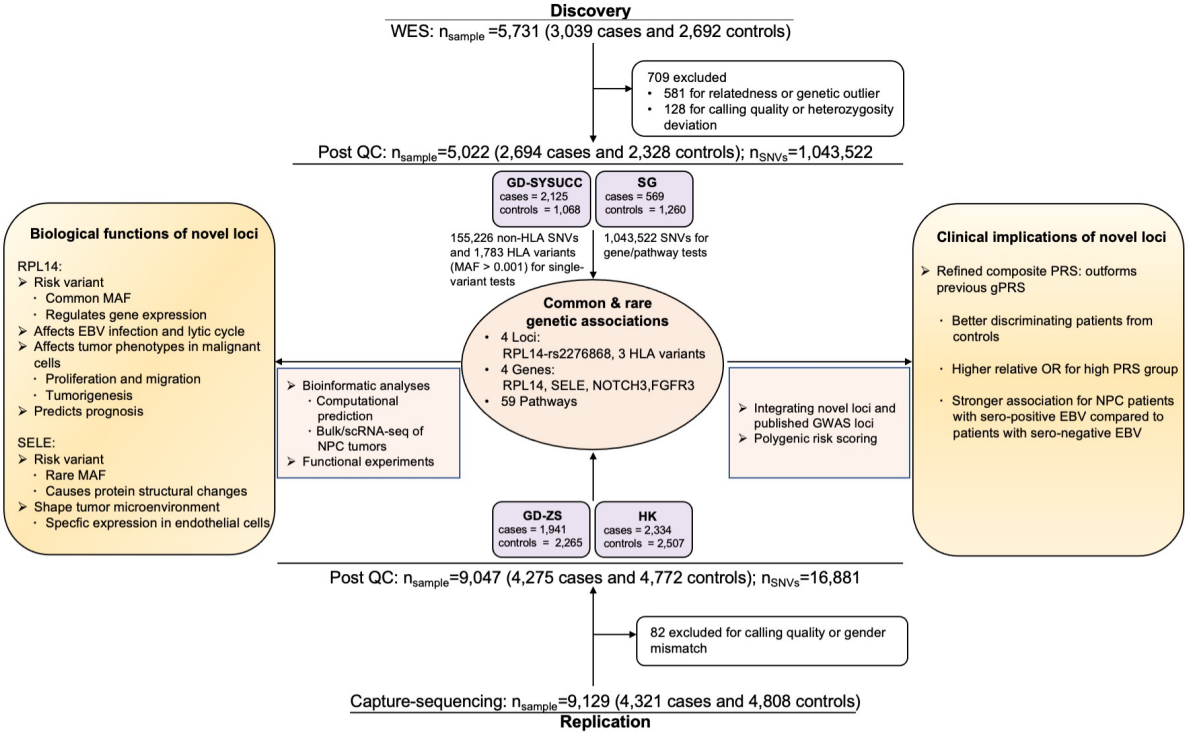

Figure 1. Study overview. A two-stage association study design was applied to investigate the genetic factors associated with NPC. In the discovery stage, a total of 5,022 samples, including the GD-SYSUCC cohort from Guangdong in China and the SG cohort from Singapore, were genotyped with WES and analyzed to identify four independent variants (two of which are novel), four novel genes, and 59 pathways associated with NPC. The associations were subsequently validated in the replication stage, which included 9,047 samples from the GD-ZS cohort in Guangdong and the HK cohort in Hong Kong, China. Bioinformatic analyses and functional experiments were conducted to explore the biological functions and the clinical implications of the novel loci.

Results

Association of single variants with NPC susceptibility

To identify susceptibility loci of NPC at single variant level, we first performed whole-exome sequencing (WES) on genomic DNA samples for the discovery stage, involving 2,694 NPC cases and 2,328 healthy controls of Han Chinese descent from southern China (GD-SYSUCC) and Singapore (SG; see Methods, **Figure 1**). After stringent quality controls, we obtained 1,043,522 single nucleotide variants (SNVs), including 362,993 potentially functional or pathogenic variants (Methods) and 335,163 novel variants which were not present in the 1000 genome phase 3, gnomAD exome, and genome database[34,35].

168 Subsequently, we performed a single-variant-based exome-wide association study (EWAS)
169 on 155,226 non-HLA SNVs and 1,783 HLA variants (including HLA alleles, amino acids [AA],
170 and SNVs) with a MAF >= 0.001 among 2,694 NPC cases (all NPC cases, ALLNPC) and
171 2,328 controls, as well as 409 NPC cases with a family history (FHNPC) and the same set of
172 controls. We observed neither evidence of genomic inflation of the associations (λ_{ALLNPC}=1.07,
173 λ_{FHNPC}=0.89, **Figure S1A**) nor significant genetic substructure between case and control
174 groups (**Figure S2**). The EWAS results revealed a total of 242 variants associated with NPC
175 risk in the ALLNPC group and 128 variants associated with NPC risk in the FHNPC group,
176 surpassing the Bonferroni significant threshold for multiple testing correction ($P < 3.2 \times 10^{-7}$;
177 **Figure S1B**). Notably, we discovered a novel non-HLA locus with several significant
178 associated SNVs (**Figure S1B**). The sentinel SNV rs2276868, located at the 5'-untranslated
179 region (5'-UTR) of the ribosomal gene *RPL14*, exhibited the strongest associations in both the
180 FHNPC (P_{FHNPC}=2.3 × 10^{-8}, Odds Ratio (OR) $_{FHNPC}$ =1.575, 95% Confident Interval (CI)
181 =1.343-1.846) and the ALLNPC groups (P_{ALLNPC}=4.2 × 10^{-7}, OR_{ALLNPC} =1.242, 95%CI=1.142-
182 1.351; **Table 1, Figure S1B**). Furthermore, the association was stronger in the family cases
183 than in the sporadic cases ($OR_{sporadic_NPC}$ =1.200, 95%CI =1.097-1.313), indicating a robust
184 genetic predisposition to NPC. Conditional analysis revealed that all associations at the *RPL14*
185 locus vanished upon adjusting for rs2276868, suggesting that this variant explains all the
186 observed associations (**Table S1, S2**). Beyond the non-HLA locus, we also identified HLA
187 variants significantly associated with NPC (**Figure S1B**). Stepwise conditional analysis
188 localized three independently associated variants, including *HLA-DQB1*03:01:01*, *HLA-A:*
189 *A_62_Q*, and rs1050462 at HLA-B (**Tables 1, Table S1**). Except for the two known
190 associations at *HLA-A: A_62_Q* and *HLA-DQB1*03:01:01*[18,36], the association of rs1050462
191 with NPC is a novel discovery whose signal is not attributed to previously reported *HLA*
192 variants [8,10,11] (see Methods; $P \leq 3.23 \times 10^{-5}$; **Table S3**), according to an additional conditional
193 analysis using an extended GD-SYSUCC cohort consisting of 1,583 cases and 3,049 controls
194 with GWAS array data [17].

195 We next conducted validations of the identified associations using two independent
196 replication cohorts consisting of 9,047 samples of Southern Chinese recruited from Hong Kong
197 (HK; 2,334 cases and 2,507 controls) and Guangdong (GD-ZS; 1,941 cases and 2,265 controls)
198 in China (see Methods). We genotyped the samples using Cap-seq to target the genomic
199 regions spanning the above variants. Meta-analysis across the replication samples consistently
200 confirmed the associations of the four variants in *RPL14* and *HLA* loci ($P_{meta} < 0.05$; **Table 1**).

201 Moreover, when combining the discovery and replication samples, the meta-analysis revealed
202 that the four variants in *RPL14* and *HLA* loci were significantly associated with NPC risk,
203 surpassing the threshold for genome-wide significance ($P < 5 \times 10^{-8}$; **Table 1**).

204

205 ***Association of genes and pathways with NPC susceptibility***

206 To identify the cumulative genetic effects of both rare and common variants within individual
207 genes on the risks of NPC, we conducted a gene-based association analysis in the discovery
208 dataset using an ensemble method that incorporates four algorithms simultaneously (see
209 Methods). For each gene, we performed separate tests that use all SNVs within the genic region
210 or only consider coding-affecting SNVs of that gene. Our analysis revealed a significant
211 association between *RPL14* and NPC, with statistical significance surpassing Bonferroni
212 threshold for multiple testing correction ($P < 2.3 \times 10^{-6}$, **Table 2**). Additionally, we validated
213 previous associations in several genes (**Table S4**).

214 We further performed a pathway-based analysis to explore the cumulative genetic effects
215 of genes involved in 6,204 curated molecular pathways in the discovery dataset (see Methods).
216 This analysis identified a total of 59 pathways associated with NPC in either the ALLNPC or
217 FHNPC groups, adhering to the false discovery rate (FDR) threshold set for multiple testing
218 correction ($P < 3.09 \times 10^{-4}$; **Figure 2A, Table S5)**. Among these pathways, we observed that
219 11 sentinel pathway genes were involved in at least two NPC-associated pathways and
220 exhibited an association with NPC in gene-based test with a significant threshold of $P < 0.01$
221 (**Figure 2B**). Notably, *SELE, NOTCH3*, and *FGFR3* had strong associations with NPC ($P <$
222 1×10^{-4}; **Figure 2B**). *SELE* was particularly outstanding, with the strongest association with
223 NPC ($P_{SELE} = 2.69 \times 10^{-6}$) and the involvement in the largest number of NPC-associated
224 pathways (**Figure 2B**).

225 To validate the associations for the significant gene *RPL14* and the top three sentinel
226 pathways genes (*SELE*, *FGFR3*, and *NOTCH3*), we re-sequenced exon regions of these four
227 candidate genes in the replication cohorts ($n_{GD\text{-}ZS}$=4,206 and n_{HK}=4,841). Gene-based
228 association analyses statistically validated all the candidate genes in the replication dataset
229 ($P_{RPL14}=1.23 \times 10^{-7}$**,** $P_{SELE}=4.05 \times 10^{-4}$**,** $P_{NOTCH3}=3.28 \times 10^{-6}$, and $P_{FGFR3}=8.96 \times 10^{-4}$; **Table 2**).
230 The association for *RPL14* was particularly robust across all replication cohorts ($P_{GD\text{-}ZS}=3.50$
231 $\times 10^{-6}$ and $P_{HK}=8.44 \times 10^{-5}$), whereas the associations for *SELE*, *NOTCH3*, and *FGFR3* were
232 more prominent in the GD-ZS cohort (**Table 2**).

233 **Table 1. Association of single variants with NPC susceptibility**

Variants information				Discovery (2,694 cases and 2,328 controls)				Replication (4,275 cases and 4,772 controls)					Combined samples (6,969 cases and 7,100 controls)		
Variant ID	CHR	A1	Gene	ALLNPC: OR (95% CI)	P	FHNPC: OR (95% CI)	P	OR (95% CI) HK (2,334 cases and 2,507 controls)	OR (95% CI) GD-ZS (1,941 cases and 2,265 controls)	OR_{meta}: (95% CI)	P_{meta}	I_{meta}^2	OR_{meta} (95% CI)	P_{meta}	I_{meta}^2
rs2276868	3	T	*RPL14*	1.242 (1.142-1.351)	4.16E-07	1.575 (1.343-1.846)	2.30E-08	1.253 (1.154-1.36)	1.193 (1.091-1.305)	1.225 (1.153-1.302)	5.26E-11	0.00	1.231 (1.172-1.293)	1.22E-16	0.00
DQB1*03:01:01	6	Present	*HLA-DQB1*	0.633 (0.568-0.705)	1.00E-16	0.585 (0.467-0.734)	3.64E-06	0.694 (0.622-0.774)	0.589 (0.522-0.663)	0.640 (0.545-0.752)	5.56E-08	74.84	0.638 (0.582-0.700)	9.43E-22	50.44
A_62_Q	6	Present	*HLA-A*	0.507 (0.462-0.556)	4.61E-47	0.483 (0.401-0.581)	1.20E-14	0.585 (0.532-0.642)	0.560 (0.505-0.621)	0.573 (0.535-0.615)	1.73E-55	0.00	0.549 (0.504-0.598)	4.69E-43	57.52
rs1050462	6	G	*HLA-B*	0.646 (0.585-0.713)	7.58E-18	0.637 (0.521-0.779)	1.08E-05	0.568 (0.513-0.629)	0.588 (0.526-0.658)	0.577 (0.535-0.622)	1.92E-46	0.00	0.600 (0.555-0.649)	2.55E-37	40.86

234 Notes: CHR, chromosome; A1, target allele/amino acid; OR (95%CI), odds ratio estimate and the 95% confidence interval; I^2, the proportion of the variance
235 in observed effect is due to variance in true effects rather than sampling error; Meta, meta-analyzed using the random effects model.

236

237 **Table 2. Associations of individual genes with NPC susceptibility**

Gene	Discovery (2,694 cases and 2,328 controls)				Replication (4,275 cases and 4,772 controls)				Combined samples (6,969 cases and 7,100 controls)
Name	Significant in tests	SNV group	Method	P	P (GD-ZS; 1,941 cases and 2,265 controls)	P (HK; 2,334 cases and 2,507 controls)	P_{meta}	Adjusted P_{meta}	P_{meta}
RPL14	Gene association	ALLSNV	SKAT (C+R)	2.17E-06	3.50E-06	8.44E-05	1.23E-07	6.16E-07	1.79E-10
SELE	Sentinel pathway genes	ALLSNV	SKAT (C+R)	2.69E-06	1.01E-03	3.94E-02	4.05E-04	2.02E-03	1.44E-07
SELE	Sentinel pathway genes	coding affecting SNV	SKAT (C+R)	3.61E-06	1.36E-03	1.20E-01	1.40E-03	7.00E-03	4.63E-07
FGFR3	Sentinel pathway genes	ALLSNV	Burden	1.24E-04	7.40E-04	1.28E-01	8.96E-04	4.48E-03	3.64E-06
NOTCH3	Sentinel pathway genes	ALLSNV	SKAT (C+R)	3.60E-04	6.00E-06	1.07E-02	3.28E-06	1.64E-05	5.41E-08

238 Notes: ALLSNV, all SNVs; SKAT (C+R), SNP-set (Sequence) Kernel Association Test for the combined effect of common (C) and rare (R) variants; Burden,
239 burden test; Meta, meta-analyzed using the summation of logits method; Adjusted P, the P value adjusted using the FDR method.

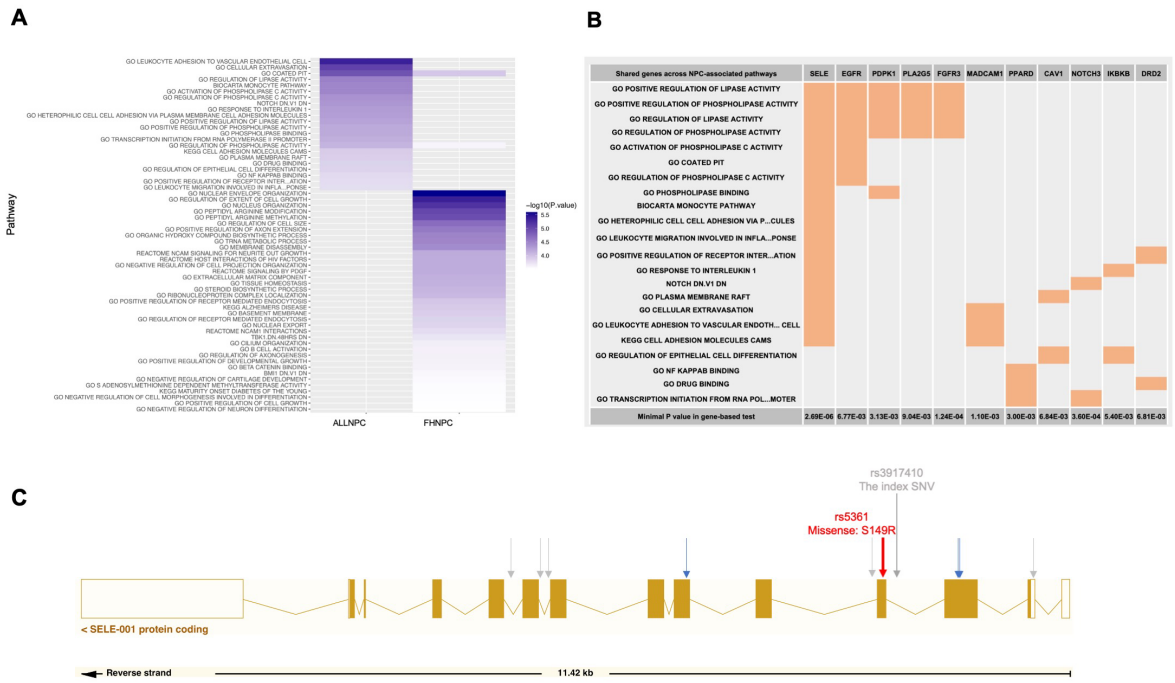

Figure 2. Significant pathways and sentinel genes associated with NPC. A. Significant pathways associated with NPC. ALLNPC denotes all NPC samples in the discovery stage, whereas FHNPC represents NPC cases with a familial NPC history. Color bars from white to purple indicate minus log-transformed P values. **B**. Sentinel genes for NPC-associated pathways. Genes indicated atop are highlighted in orange if they are part of a specific pathway. The listed genes are those belonging to at least two NPC-associated pathways and exhibiting a gene-based association P value below 0.01. **C**. Locations of the rare variants associated with NPC at significance level of $P < 1\times10^{-4}$ within the genic regions of SELE. Grey arrows denote non-coding variants, blue arrows represent synonymous coding variants, and the red arrow indicates non-synonymous coding variant predicted as "deleterious". The rs5361 minor allele introduces a missense mutation at position 149, resulting in an amino acid substitution from S to R. The index SNV rs3917410 showed the most significant P value in the association tests in the discovery stage.

We next fine-mapped the variants (MAF > 0.001) contributing to the gene-level associations for the four replicated genes using the discovery dataset (n=5,022). A constituent variant was considered to have a "major" contribution if its variant-level association P value was less than 1×10^{-4}. Using this criterion, we detected a major contribution from a common variant for *RPL14* (**Table S6**), as well as major contributions from multiple rare variants for *SELE* (**Table S7**). However, no major contributing variants were detected for *FGFR3* (**Table S8**) or *NOTCH3* (**Table S9**). Specifically, among the four SNVs (MAF > 0.001) in *RPL14*, the sentinel SNV rs2276868 (MAF=0.36, $P_{SNV}=4.16 \times 10^{-7}$) and another SNV rs2276869 (MAF=0.10, $P_{SNV}=0.001$) shared modest linkage disequilibrium (LD; $R^2=0.2$) and were the

264 only two *RPL14* variants associated with NPC (P_{SNV} <0.05; **Table S6**). Removing these two
265 SNVs from the gene-based analysis diminished the gene-level association of *RPL14* with NPC
266 (P_{gene}=0.34). Controlling for rs2276868 also abolished the associations of rs2276869 (**Table**
267 **S6**). These findings suggest a predominant contribution of common variant rs2276868 to
268 *RPL14*'s association with NPC.

269 For *SELE*, a total of 23 SNVs (MAF > 0.001) were detected, including seven common
270 (MAF>=0.01) and 16 rare variants (MAF<0.01; **Table S7**). Of these, 10 SNVs were strongly
271 associated with NPC (P_{SNV}=2.68 × 10^{-5} ~ 4.98 × 10^{-5}; **Table S7**), with rs3917410 as the sentinel
272 SNV (P=2.68 × 10^{-5}) and sharing nearly complete LD with the other nine SNVs (R^2 > 0.99;
273 **Table S7**). All the 10 SNVs are rare, including one non-synonymous coding (rs5361), three
274 synonymous coding, and six non-coding variants. Controlling for rs5361 variant abolished the
275 association signals with NPC for the other rare variants in *SELE* (Adjusted P>0.05; **Table S7**).
276 The rs5361 variant is a missense mutation (T>G) in the exon 4 of *SELE* (**Figure 2C**), resulting
277 in an amino acid substitution from the conservative Serine (S) (**Figure 2C, Figure S3A**) to
278 Arginine (R) at position 149. Furthermore, multiple algorithms predicted this S149R
279 substitution as "deleterious" (Polyphen-2 score=0.997; CADD score=23; SIFT score=0;
280 REVEL score=0.516; MetaLR score=0.772; **Figure S3B**). Collectively, these findings suggest
281 that the rare variant rs5361 (*SELE*-S149R) is likely a causal variant accounting for the NPC
282 associations observed in *SELE*.

283

284 ***Functional characterization of the novel loci***

285 ***Distinct cellular expression patterns of NPC-associated genes***

286 To understand the functional consequences of the novel loci in NPC, we first investigated their
287 cellular expression patterns along with the known NPC-associated genes (**Table S10**). We
288 harnessed single-cell transcriptomic analyses of tumor samples from 56 NPC patients and
289 various non-tumor tissues from 15 donors without cancer[37] (see Methods). *RPL14* exhibited a
290 universal expression across all cell types, notably in the malignant epithelial cells (**Figure 3**).
291 Similarly, most HLA-I genes also showed broad expression in all cell types. By contrast, *SELE*
292 exhibited specific expression in endothelial cells across both tumor and non-tumor tissues
293 (**Figure 3C, Figure S4**). We also noted specific expression of some genes in cell types other
294 than the malignant epithelial cells in NPC tumors (**Figure 3**). For example, *NOTCH3* was
295 specifically expressed in cancer associated fibroblasts, while HLA-II genes were mainly

296 expressed in various stromal cell types in the tumor microenvironment (TME; **Figure 3**).
297 Additionally, by performing single-cell transcriptomic analyses of tumor samples from other
298 epithelial cancers, including lung, gastric, and colorectal cancers (see Methods), we observed
299 that gene associated with those cancers exhibited similar expression patterns observed in NPC,
300 with some expressed predominantly in epithelial cells and some predominantly in stromal cells
301 in the TME (**Figure S5**). These findings strongly indicate that genes conferring susceptibility
302 to cancers are not necessarily confined to expression in malignant cells. Instead, these genes
303 often exhibit predominant expression in diverse cell populations within the TME, suggesting a
304 crucial role of genetic impact on stromal cells in cancer development.

305

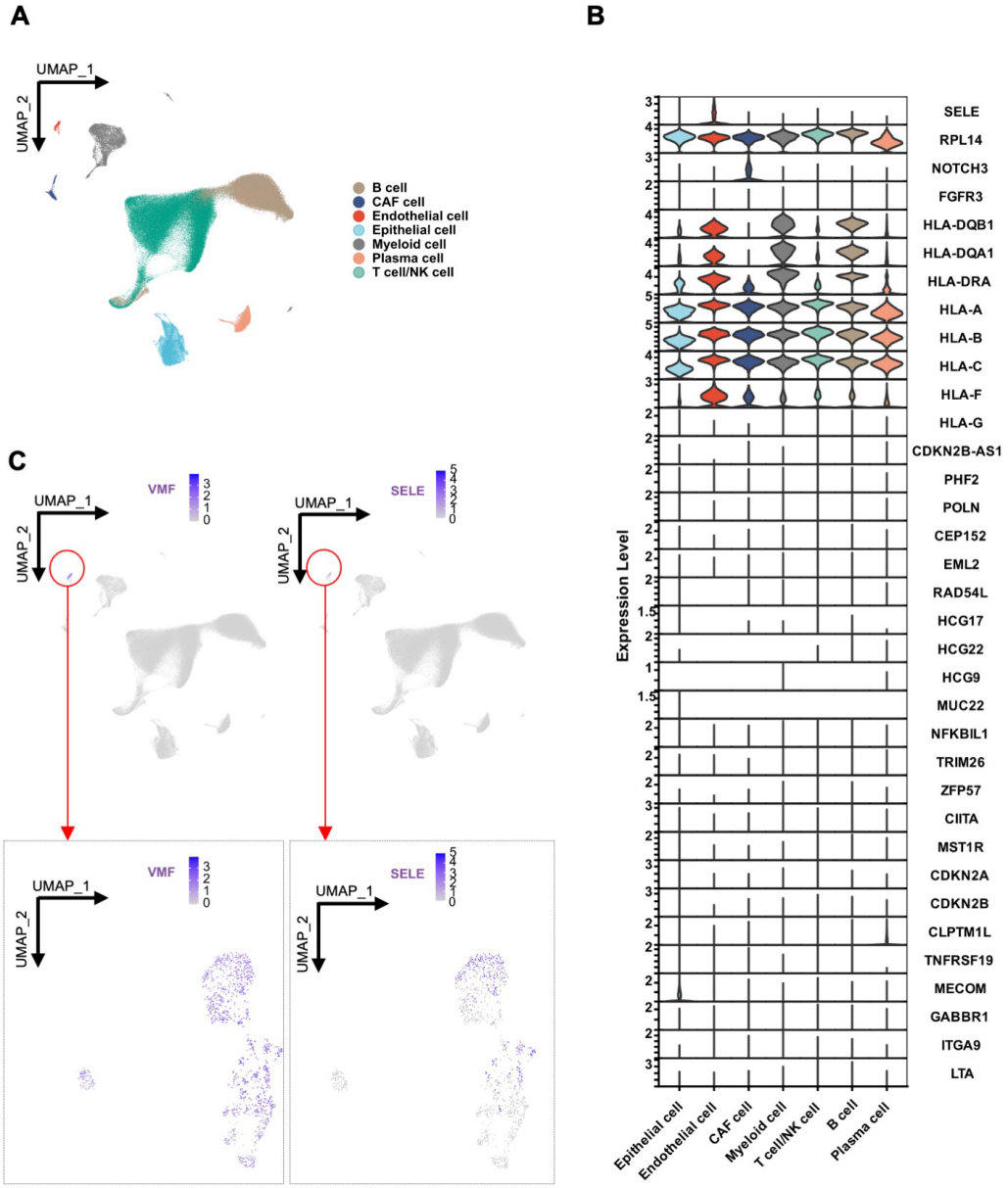

Figure 3. Expression patterns of novel and known NPC-associated genes across diverse cell types in NPC tumor tissues. Single-cell transcriptomic analyses of 223,593 cells derived from NPC tumor tissues in 56 patients. **A**. UMAP plot of 223,593 single cells grouped into seven major cell clusters. **B**. Violin plot illustrating normalized expression of NPC-associated genes across these major cell clusters. All epithelial cells captured in NPC tumor were malignant (see Methods). **C**. The expression of the marker gene (*VWF*) for endothelial cells and alongside the novel NPC-associated gene *SELE*; top panel: initial UMAP plot, bottom panel: re-normalized UMAP emphasizing cells highlighted by the red circles in the initial UMAP plot.

319 ***rs2276868 regulates RPL14 expression through the NKRF transcription factor***

320 Given the location of rs2276868 at the RPL14 promoter [38] (**Figure S6, S7A**) and the stable
321 expression of *RPL14* in malignant epithelial cells (**Figure 3**), we aimed to investigate the
322 potential regulatory role of rs2276868 in *RPL14* mRNA expression in epithelial cells. We first
323 performed a single-cell-transcriptome-based eQTL analysis using 15,623 malignant epithelial
324 cells from tumor tissues of 35 NPC patients. We observed that CC or CT genotype of
325 rs2276868 was significantly associated with a higher expression of *RPL14* in malignant NPC
326 cells compared to the TT genotype (**Figure 4A**). Subsequently, luciferase reporter assay
327 demonstrated that the rs2276868-[T] construct had significantly lower luciferase activity
328 compared to the rs2276868-[C] construct in human 293T cells (**Figure 4B**). These findings
329 strongly suggest the influence of rs2276868 on *RPL14* transcription, which may involve
330 modulating the binding affinity of certain transcription factor (TF).

331 To identify such potential TF, we conducted a comprehensive screening and identified 24
332 candidate TFs, which showed a positive correlation with the mRNA expression of *RPL14* in
333 two independent bulk transcriptomic datasets of NPC tissues (n_{Bei}=87 and n_{Zhang}=113; **Figure**
334 **4B, Figure S7B**). Subsequent siRNA screening assays confirmed that five of the 24 TFs were
335 capable of modulating *RPL14* expression (**Figure S7C**). Among them, *NKRF* knockdown
336 significantly reduced *RPL14* transcription in NPC cells (**Figure 4B, Figure S7C-E**).
337 Furthermore, knockdown or overexpression of *NKRF* exhibited a preferential effect on the
338 transcription activity of the rs2276868-[C] construct over the rs2276868-[T] construct in
339 luciferase reporter assays (**Figure 4E, F**). Consistently, single-cell transcriptome analysis
340 revealed a stronger positive correlation between the expression of *NKRF* and *RPL14* in
341 malignant NPC cells carrying the rs2276868-[C] compared to the rs2276868-[T] carriers
342 (**Figure 4J**). Moreover, chromatin immunoprecipitation (ChIP) assay demonstrated that NKRF
343 specifically binds to a refined genomic region encompassing rs2276868 (**Figure 4G-I, S7F**).
344 Taken together, these data strongly suggest that rs2276868 influences *RPL14* expression
345 through its interaction with *NKRF*, which preferentially binds to the promoter region housing
346 rs2276868-[C] to foster enhanced transcription of *RPL14* in NPC tumors.

347

348

349

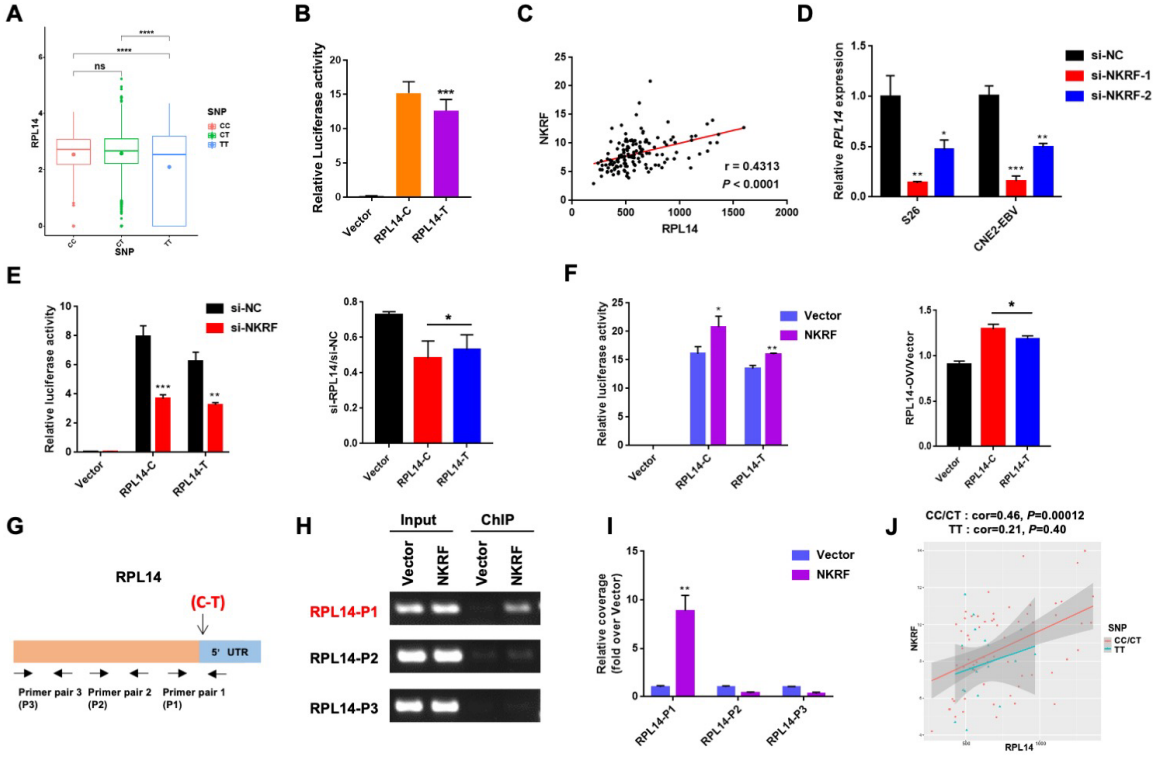

Figure 4. rs2276868 regulates the expression of *RPL14*. A. Single-cell transcriptome analysis showed the mRNA expression of RPL14 in 15,623 malignant epithelial cells from 35 NPC samples with different rs2276868 genotypes. **B**. Relative luciferase activity changes in 293T cells transfected with plasmids containing rs2276868 -[C], -[T], or control vectors. **C**. Pearson correlation analysis indicates the relationship between *RPL14* and *NKRF* expression (measured as transcript per million, TPM) in transcriptome data of NPC patients (n=87). **D**. RT-qPCR illustrates the mRNA expression of RPL14 in NPC cells transfected with NKRF siRNAs or control siRNA. **E-F**. Relative luciferase activity in 293T cells co-transfected with the rs2276868 -[C] or -[T] plasmids and NKRF siRNA (F) or NKRF overexpression vectors (G). Corresponding statistics are presented at the right. **G**. Schematic diagram indicates primer pairs used for PCR amplification of RPL14 fragments. **H-I**. ChIP assay in S26 cells transfected with Flag-NKRF and control vectors. ChIP PCR (H) and qPCR (I) showed RPL14 expression level in cells. P1-3 denote primer pairs targeting genomic regions shown in G. **J**. Pearson correlation analysis indicates the relationship between NKRF and RPL14 expression in single-cell transcriptome data are different for NPC patients with different genotypes. rs2276868 -[CC/CT] patients have a stronger correlation than rs2276868-[TT] patients. *$p < 0.05$, **$p < 0.01$, ***$p < 0.001$.

RPL14 suppresses EBV infection and lytic cycle in NPC

To investigate the role of *RPL14* in NPC development, we first examined the relationship between *RPL14* expression and the transcriptional activity scores of various molecular pathways in NPC (see details in Methods). Through REACTOME and GO analysis of malignant epithelial cells in NPC scRNA-seq data (n_{sample}=35 and n_{cell}=15,623), we observed

374 a significant association between *RPL14* and a pathway related to viral translation
375 (GO:0019081: viral translation. $P_{sc}=1.63 \times 10^{-6}$; **Figure 5A, Table S11**). Additionally,
376 REACTOME and GO analysis of bulk RNA-seq data from NPC tissues ($n_{bulk_Bei}=93$ and
377 $n_{bulk_Zhang}=113$) revealed significant associations between *RPL14* and multiple pathways
378 related to viral infection. These pathways include SARS-COV-2 modulation of host translation
379 machinery ($P_{bulk_Bei}=8.48 \times 10^{-16}$, $P_{bulk_Zhang}=9.11 \times 10^{-14}$) and influenza infection
380 ($P_{bulk_Bei}=2.00 \times 10^{-14}$, $P_{bulk_Zhang}=1.66 \times 10^{-13}$; **Figure S8; Table S12, S13**). Considering the
381 well-known involvement of EBV in NPC etiology[39], we hypothesized a potential link between
382 *RPL14* and EBV processes. Supportively, in EBV-positive malignant NPC cells, we observed
383 a significant negative association ($R= -0.27$, $P < 2.2\times10^{-16}$) between *RPL14* expression and the
384 EBV activity score, a metric developed by consolidating expression levels of multiple EBV
385 genes (see Methods; **Figure 5B**). Furthermore, rs2276868-[T] carriers exhibited decreased
386 *RPL14* expression but increased expression of EBV latent genes *LMP1* and *LMP2* as compared
387 to rs2276868-[C] carriers in the same cell group (**Figure 5C**). These results corroborate the
388 connection between *RPL14* and EBV-driven processes.

389 To further explore the interaction between *RPL14* and EBV, we monitored the protein
390 expression of RPL14 in NPC cells post EBV infection over different timepoints. We observed
391 a significant downtrend in RPL14 expression concurrent with EBV infection (**Figure 5D**). By
392 contrast, RPL14 knockdown resulted in a significant rise in EBV infection in NPC cells, while
393 RPL14 overexpression led to a marked reduction in EBV infection (**Figure 5E-H**). We also
394 noticed a decline in RPL14 expression when EBV lytic cycle was induced using TPA and NaB
395 in NPC cells (**Figure 5I, J; Figure S9**). Furthermore, RPL14 knockdown remarkably
396 augmented the expression of EBV lytic genes in NPC cells, while RPL14 overexpression
397 significantly reduced their expression (**Figure 5K, L**). These observations strongly suggest that
398 RPL14 acts as a suppressor of EBV infection and lytic cycle in NPC.

399

400

401

402

403

404

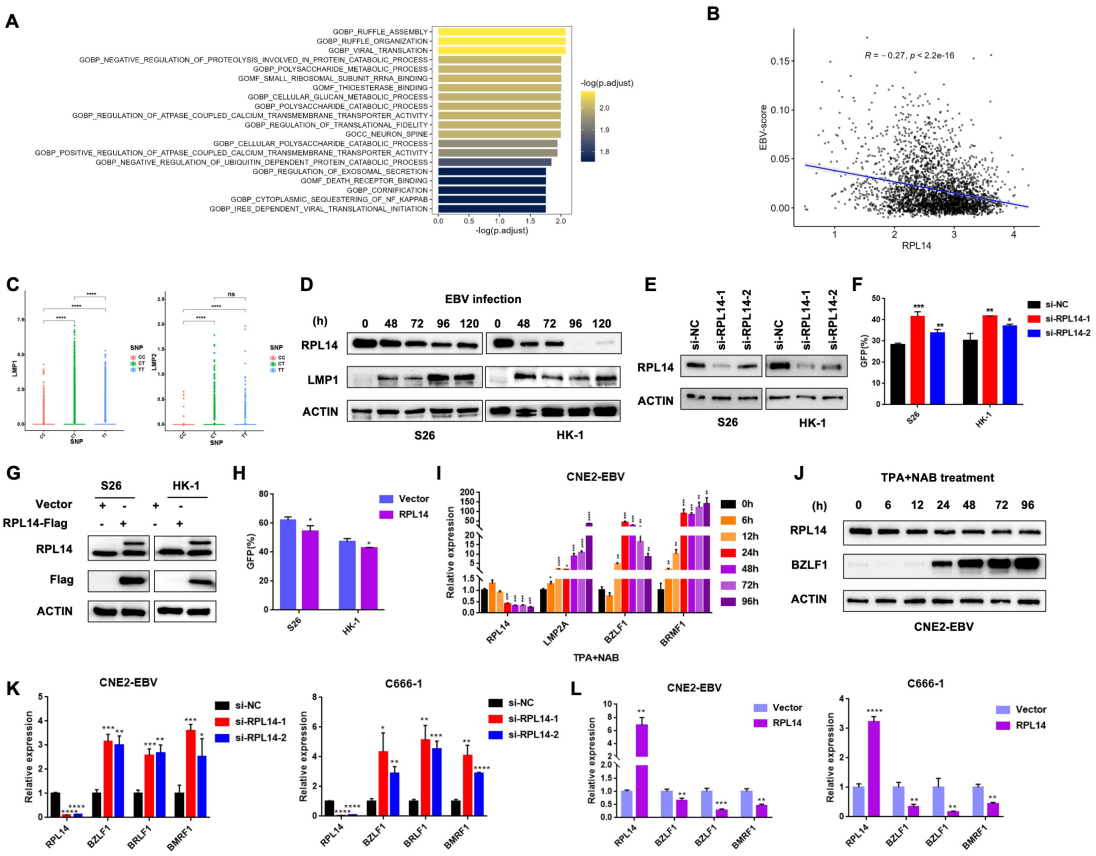

Figure 5. *RPL14* inhibits EBV infection and lytic cycle activation in NPC cells. A. The top 20 pathways significantly associated with RPL14 expression in malignant epithelial cells from NPC tumor. **B.** Correlation analysis between EBV-activity scores and *RPL14* expression within malignant epithelial cells. **C.** Single-cell transcriptome analysis showing *LMP1* and *LMP2* expression in NPC samples with either rs2276868 -[C] or -[T] genotypes. **D.** Western blot examination of RPL14 and LMP1 protein levels in NPC cell lines S26 and HK-1 cells infected with EBV at different timepoints. **E.** Western blot assessment of the knockdown efficiency of RPL14 siRNAs or control siRNA in S26 and HK-1 cells. **F.** Flow cytometry quantification of GFP intensity for the EBV infection efficiency in the NPC cells described in E. **G.** Western blot assay showing RPL14 protein expression in S26 and HK-1 cells infected with lentivirus stably expressing RPL14. ACTIN served as a loading control. **H.** Flow cytometry assessment of EBV infection efficiency in the cells described in G. **I-J.** Changes of gene expression in CNE2-EBV cells subjected to EBV lytic induction with TPA and NAB. RT-qPCR (I) and western blotting (J) were performed to detect the mRNA and protein expression, respectively, of RPL14 and EBV genes at different timepoints of EBV lytic induction. **K-L.** RT-qPCR analysis of EBV lytic gene expression in CNE2-EBV and C666-1 cells transfected with RPL14 siRNAs or control siRNA (K), or infected with lentivirus stably expressing RPL14 vector or control vector (L). $*p < 0.05$, $**p < 0.01$, $***p < 0.001$, $***p < 0.0001$.

RPL14 impedes tumorigenesis in NPC cells

We next explored the function of *RPL14* in NPC tumorigenesis. We first manipulated *RPL14* expression in an *in vitro* NPC cell model (**Figure 6A; S10A**). Cell growth curves and colony

428 formation assays revealed that the stable overexpression of *RPL14* significantly inhibited NPC
429 cell proliferation. Conversely, stable knockdown of *RPL14* had an opposite effect, promoting
430 proliferation (**Figure 6B-C, Figure S10B-C**). Transwell assays revealed that *RPL14*
431 overexpression suppressed NPC cell migration, while its knockdown enhanced the migration
432 (**Figure 6D; Figure S10D**). These observations strongly suggest that *RPL14* inhibits the
433 tumorigenesis of NPC cells.

434

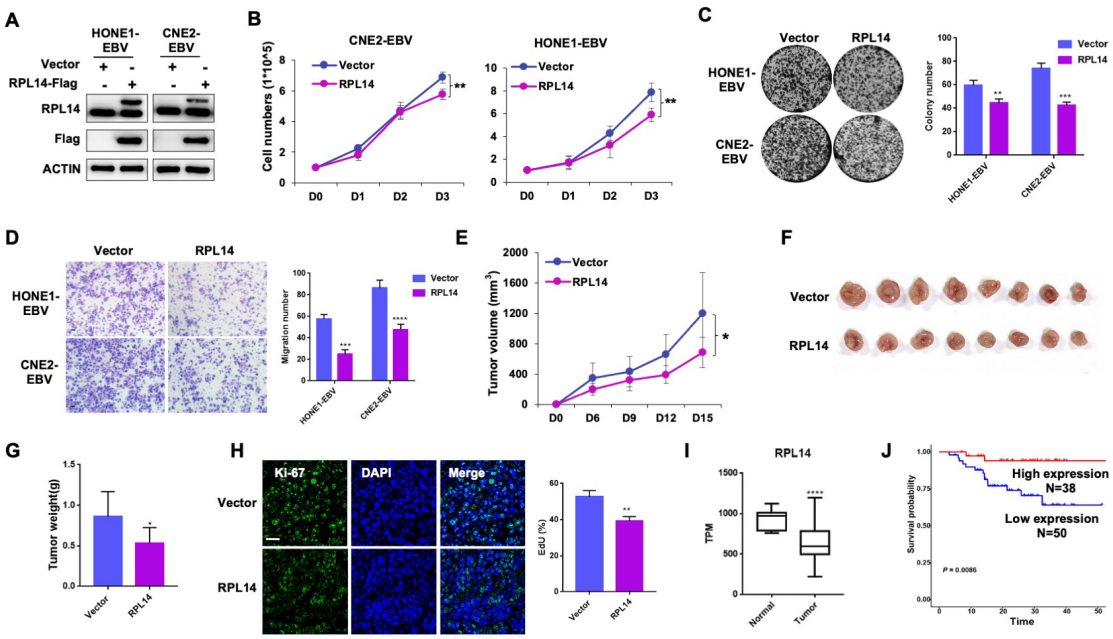

435

436 **Figure 6. Tumor suppressive function of *RPL14* in NPC. A**. Western blot analysis showing
437 RPL14 protein levels in NPC cells infected with RPL14 overexpressing lentivirus. ACTIN
438 serves as the loading control. **B**. Cell growth curves of the cells described in A. **C**. Colony
439 formation assay for the cells described in A. Corresponding statistical analysis is shown to the
440 right. **D**. Transwell migration assay evaluating the migration ability of the cells described in A.
441 The statistical analysis is presented on the right. **E-H**. Tumor growth evaluation in a nude mice
442 model with subcutaneous injection of NPC cells described in A. Tumor volumes were
443 measured every three days. Visual presentation of tumor post-sacrifice (F) and weight (G) were
444 presented. IF detection of Ki-67 expression (H) in the tumors described in F, and the
445 corresponding statistical analysis is shown on the right. **I**. Transcriptomic analysis showcasing
446 mRNA levels of RPL14 in NPC (n=87) versus control samples (n=10). **J**. Kaplan-Meier
447 survival analysis linking RPL14 expression to survival time in NPC patients using bulk RNA-
448 seq data (n=88). $*p < 0.05$, $**p < 0.01$, $***p < 0.001$, $****p < 0.0001$.

449

450 To corroborate the tumor-suppressive function of *RPL14 in vivo*, we established a mouse
451 model with subcutaneous injection of NPC cells stably expressing *RPL14*. We observed a
452 significant inhibition on tumorigenesis as reflected by the diminished tumor volume and weight

453 in mice with *RPL14* overexpression compared to the control group (**Figure 6E-G**).
454 Supportively, immunofluorescence staining of Ki-67, a proliferation marker, revealed a
455 substantial decrease in Ki-67 positive cells in the *RPL14*-overexpressing tumors compared to
456 the control tumors (**Figure 6H**). Furthermore, we observed a significant lower expression of
457 *RPL14* in NPC tissues compared to nasopharyngeal tissues from individuals with rhinitis
458 (**Figure 6I**). Kaplan-Meier survival analysis revealed that low expression of *RPL14* was
459 significantly correlated with a poor prognosis of NPC patient (**Figure 6I**). These findings
460 strongly suggest *RPL14* as a tumor suppressor in NPC.

461

462 ***SELE-S149R promotes NPC development through gain of function in endothelial cells***

463 *SELE* encodes E-selectin, a selectin cell adhesion molecule specifically expressed on the
464 surface of endothelial cells (**Figure 3C**). E-selectin plays a pivotal role in attracting cancer
465 cells by binding to ligands like glycoproteins[40]. Structural modeling of E-selectin paired with
466 glycomimetic antagonist ligand revealed that the Ser149 residue of SELE, implicated in the
467 rs5361 variant, is in close proximity to its ligand, and the S149R substitution (**Figure 2C**) leads
468 to an extension of E-selectin's side chain, potentially altering its interaction with glycoproteins
469 (**Figure 7A**). This aligns with a previous finding that *SELE*-S149R introduces a gain-of-
470 function effect on the recruiting capability of E-Selectin[41].

471 To probe the functional implications of the *SELE*-S149R mutation in the context of NPC,
472 we developed a model using human umbilical vein endothelial cells (HUVECs) stably
473 overexpressing either the wild-type SELE (*SELE*-Ser149, SELE-WT) or its S149R mutant
474 variant (SELE-MUT, **Figure 7B**). Transwell assays revealed that overexpression of SELE,
475 especially the SELE-MUT, significantly boosted the migration ability of HUVEC cells (**Figure**
476 **7C**). Tube formation assay further demonstrated that SELE, particularly the mutant form,
477 markedly enhanced the endothelial cell's ability to form capillary-like structures, (**Figure 7D**),
478 indicating a gain-of-function effect of the S149R mutation in promoting angiogenesis. We next
479 employed a co-culture model involving HUVECs (expressing either SELE-WT or MUT) and
480 NPC cell lines (HK-1 and S26). Strikingly, HUVECs overexpressing SELE, especially the
481 SELE-MUT variant, substantially increased the migration of NPC cells (**Figure 7E**). This was
482 further substantiated by *in vivo* xenograft assays, which showed increased tumorigenesis in
483 NPC cells co-cultured with HUVEC-SELE-MUT, evident from the augmented tumor volume
484 and weight (**Figure 7F-H**). Moreover, IHC staining of CD34, a marker of vessels, revealed

485 that SELE-MUT overexpression significantly promote the angiogenesis *in vivo* (**Figure 7I**).
486 Furthermore, lymph node metastasis assays reinforced these findings, demonstrating that co-
487 culture with HUVEC-SELE-MUT cells substantially promoted the metastasis of NPC cells
488 (**Figure 7J-L**). These results strongly suggest that *SELE*-S149R mutation in endothelial cells
489 plays a crucial role in escalating both tumorigenesis and metastasis in NPC cells.

490

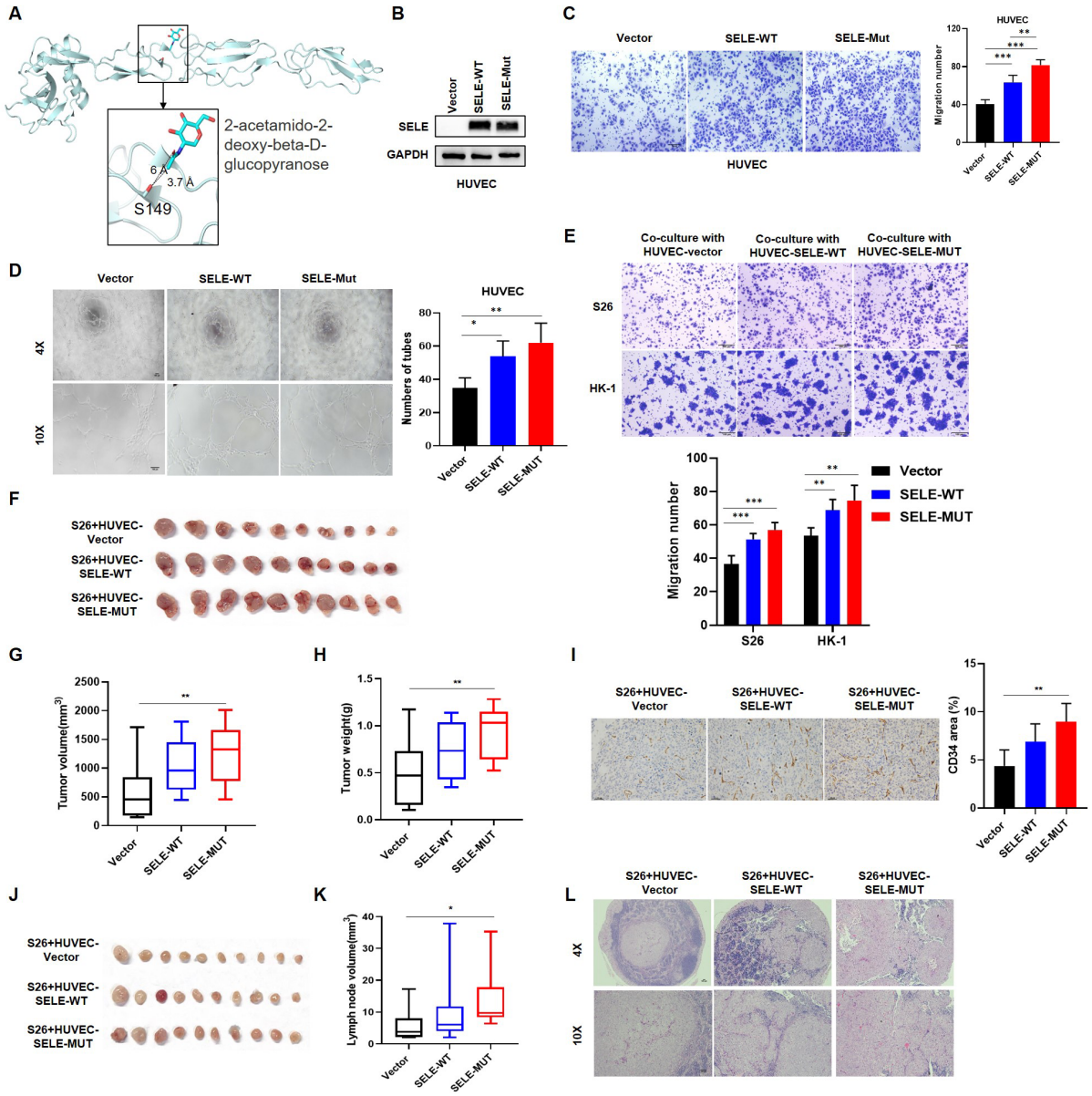

491

492 **Figure 7. SELE-S149R mutation in endothelial cells promotes the tumorigenesis and**
493 **metastasis of NPC cells. A.** Structure prediction of E-selection paired with glycomimetic
494 antagonist ligand 2-acetamido-2-deoxy-beta-D-glucopyranose (PDB code 4C16). The spatial
495 proximity between Ser149 and the ligand is highlighted. Both the Ser149 side chain and the
496 ligand are shown as sticks, with the distances between the OG atom of Ser149 and the C8 or
497 O7 atoms of the ligand specified. **B.** Western blot examination of SELE protein level in
498 HUVEC cells infected with lentivirus overexpressing SELE-WT, S149R mutant or control

499 vectors. **C.** Transwell migration assay evaluating the migration ability of the cells described in
500 B, with statistical analysis presented at the bottom. Scale bar, 100 μm. **D.** Tube formation assay
501 with cells described in B. The statistical analysis is presented on the right. Scale bar, 100 μm.
502 **E.** Transwell migration assay assessing the migration ability of the NPC cell lines (S26 and
503 HK-1) co-cultured with HUVEC cells from B (S26/HK-1: HUVEC = 10:1), accompanied by
504 statistical analysis presented at the bottom. Scale bar, 200 μm. **F-H.** Tumor growth evaluation
505 in xenograft model with subcutaneous injection of S26 cells described in E. Tumor volumes.
506 (G) are measured and visual presentation of tumor post-sacrifice (F) and weight (H) are
507 presented. **I.** IHC staining of CD34 in tumors presented in F. The statistical analysis is
508 presented on the right. Scale bar, 100 μm. **J-L.** Tumor lymphatic metastasis of S26 cells
509 described in E. Lymph nodes are visualized (I) and measured (J), with HE staining conducted
510 to assess metastasis in these lymph nodes (K). Scale bar, 100 μm. $*p < 0.05$, $**p < 0.01$, $***p$
511 < 0.001.

512

513 ***Genetic contributions of common and rare variants to NPC susceptibility***

514 We next undertook a comprehensive analysis to quantify the overall heritability of NPC
515 explained by SNVs derived from WES, which was further broken down based on the MAF and
516 LD score classifications of these SNVs, using GREML-LDMS model (see Methods). We
517 observed that a total of 15.2% of NPC susceptibility (with a standard error of 3.6%) could be
518 explained by the genetic effects of all WES-derived SNVs, including 4.4% and 10.8%
519 attributed to variants within the HLA and non-HLA regions, respectively. Notably, rare
520 variants (MAF < 0.01) in the non-HLA regions explained a substantial 82.4% of the WES
521 SNV-heritability (**Figure 8A**). Furthermore, variants with the lowest LD scores, meaning
522 relative independence, contributed the largest proportion (30.6%) to the WES SNV-heritability
523 (**Figure 8A**).

524 Through a comparative analysis using a joint model that considers multiple genetic risk
525 factors simultaneously (see Methods), we further revealed that the minor allele G of the rare
526 variant *SELE*-rs5361 conferred a substantial disease risk (OR=2.20~2.22, **Figure S11**) in the
527 two Guangdong cohorts (GD-SYSUCC and GD-ZS). This risk level is comparable to that
528 associated with the highest 20% of the population's polygenic risk score (PRS) derived from
529 HLA variants (OR=2.14~2.30, **Figure S11**). Intriguingly, the risk also overshadowed that
530 conferred by the minor allele T of the common variant *RPL14*-rs2276868 (OR = 1.22~1.45) or
531 the highest 20% of the population's PRS for NPC from non-HLA GWAS variants (OR = 1.31-
532 1.80, **Figure S11**). Additionally, by assessing the phenotypic variance ascribed to each locus[42],
533 we also revealed that HLA loci are predominantly responsible for the NPC phenotypic variance,
534 while the *RPL14* common variant significantly explain a greater portion of disease variance
535 than the *SELE* rare variant (**Figure S11**).

536

537 ***Polygenic risk prediction improved by novel loci and mediated by EBV infection***

538 To assess the efficacy of the novel loci in predicting NPC risk, we developed a refined
539 composite polygenic risk score (rcPRS) that simultaneously considers NPC-associated SNVs
540 and the leading SNVs in NPC-associated genes and pathways identified in our study and
541 previous GWASs (see Methods; **Table S15**). Notably, the rsPRS demonstrated a consistent
542 right-skewed distribution for NPC cases compared to controls across all discovery and
543 replication datasets (**Figure 8B**), suggesting a higher predictive value of rsPRS in identifying
544 individuals at risk. Furthermore, the rcPRS achieved an area under curve (AUC) for risk
545 prediction ranging between 0.659 and 0.666 in the GD-SYSUCC discovery and replication
546 samples, outperforming the published GWAS-based PRS in the GD-SYSUCC sample (gPRS;
547 AUC = 0.649; **Figure 8C; see Methods**)[10]. This improvement in predictive accuracy is largely
548 attributable to the inclusion of two novel common variants, rs1050462 in *HLA-B* and
549 rs2276868 in *RPL14*, as evidenced by our leave-one-out analysis (**Table S16**). Further
550 stratification of individuals based on their NPC PRSs, either rcPRSs or gPRSs, revealed a more
551 pronounced rising trend in the relative disease risk with the escalating rcPRS compared to the
552 gPRS (**Figure 8D**). Individuals in the highest percentile rage (95-100%) of the rcPRS exhibited
553 approximately double the relative risk (OR_{rcPRS_discov}=15.1) than those with the gPRS
554 (OR_{gPRS_discov}=8.4; **Figure 8D**). These findings suggest that incorporating novel loci into the
555 rcPRS not only improves its accuracy in distinguishing disease risk but also enhances its
556 capability to stratify individuals based on their likelihood to develop NPC.

557 Noteworthily, in a subset of 1,018 cases and 774 controls from the GD-SYSUCC cohort
558 that had data on serological antibody against the EBV-encoded virus capsule antigen (EBV
559 VCA-IgA), we observed a stronger association between rcPRS and NPC susceptibility in
560 individuals tested seropositive for EBV VCA-IgA compared to those tested seronegative
561 **(Figure 8E)**. Interaction analysis statistically further confirmed that the association between
562 the rcPRS and NPC disease status was significantly mediated by EBV status ($P_{interaction}$=0.03).
563 These findings suggest that the polygenic risk of NPC is mediated by serum EBV activity, and
564 that rcPRS may have a greater utility in predicting NPC risk among individuals with serological
565 evidence of EBV infection.

566

567

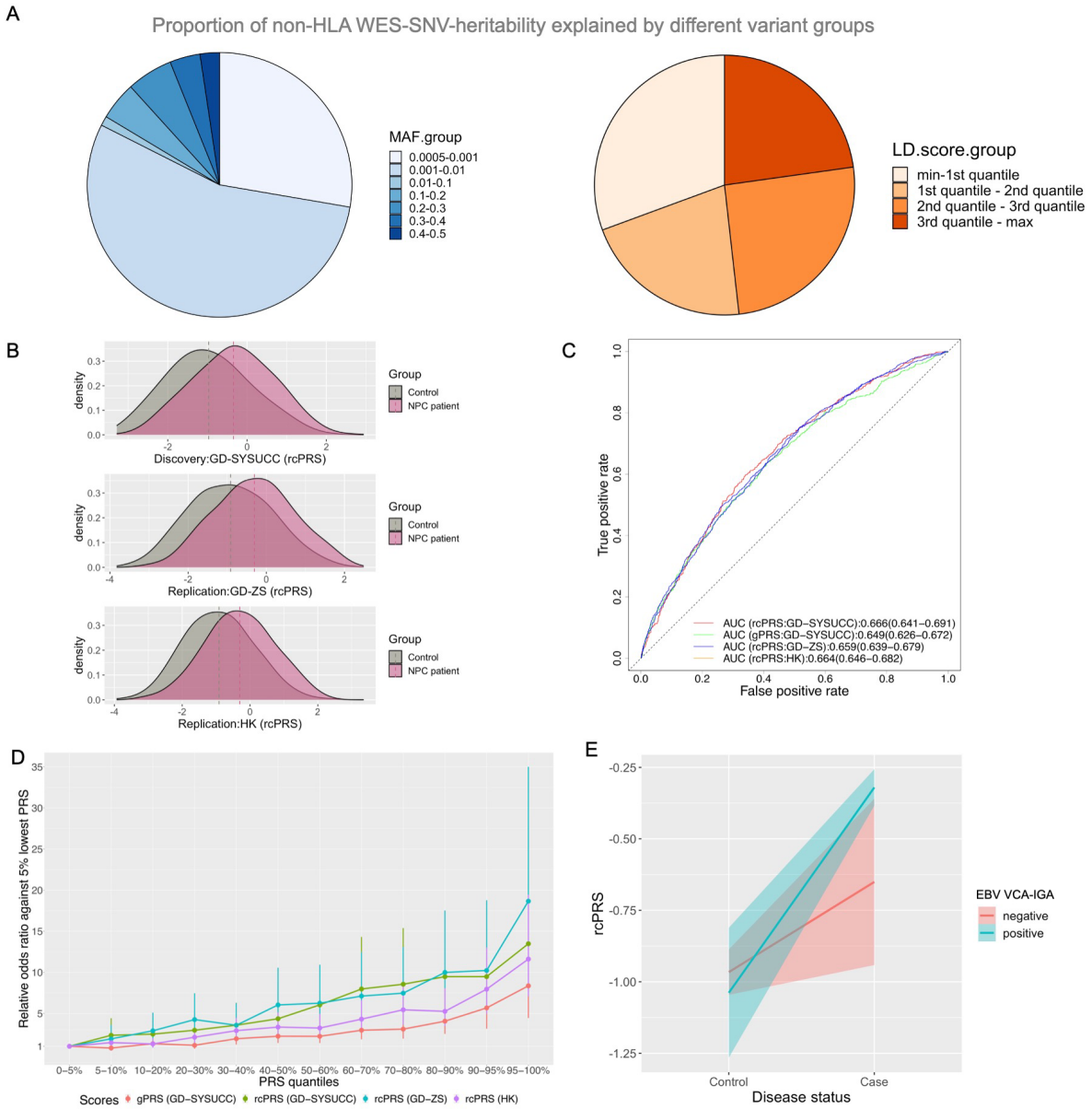

Figure 8. Contribution of common and rare variants to NPC susceptibility. A. Fractional representation of NPC heritability attributable to non-HLA WES-SNVs, categorized by minor allele frequency (MAF) and linkage disequilibrium (LD). For each variant, MAF was calculated using the discovery samples, and LD score represented the aggregated R^2 with adjacent variants spanning a 200kb window. **B**. Density plots illustrating the PRS incorporating the novel loci and previously known GWAS loci (refined composite PRS, rcPRS) for cases and controls in both the discovery and replication cohorts. **C**. Receiver operating characteristic curves comparing the rcPRS and previously reported GWAS PRS (gPRS) for NPC across different cohorts. **D**. Relative odds ratio comparing the rcPRS or gPRS bins and the 5% lowest quantile group in different cohorts. **E**. Correlation of rcPRS with disease status in individuals categorized by their EBV VCA-IgA status.

582 **Discussion**

583 Here we conducted the largest whole-exome sequencing association study on NPC to date and
584 unveiled three novel variants linked to NPC susceptibility, including the common variant
585 rs2276868 in the promoter (5'-UTR) region of *RPL14*, the rare coding variant rs5361 in *SELE*,
586 and another common variant rs1050462 in HLA-B locus[8,11]. Notably, the identification of the
587 *RPL14* locus underscores the significant role of familial history in NPC. This mirrors patterns
588 observed in other complex diseases[42], suggesting both genetic or environmental factors related
589 to family history might amplify the genetic impact of individual variants on NPC risk. A
590 possible explanation for this locus remaining undetected earlier could be its pronounced genetic
591 risk in familial cases (OR_{FHNPC} =1.575) compared to sporadic cases ($OR_{sporadic_NPC}$ = 1.200),
592 coupled with the vast sample size of our study. Additionally, the successful replication of
593 associations with *SELE* and other two sentinel pathway genes underlines an efficient approach
594 to identify and decompose disease associations at the pathway level.

595 Our study sheds light on the functional roles of the novel genes, offering a better
596 understanding of the pathogenic mechanisms underlying NPC. We uncovered that the variant
597 rs2276868 modulates *RPL14* expression through the transcription factor *NKRF*, which is an
598 inhibitor to the NF-κB pathway involved in NPC development[43,44]. Single-cell transcriptomic
599 analyses revealed an inverse association between *RPL14* expression and EBV activity in
600 malignant NPC cells, which is further corroborated by the suppressive effect of RPL14 on EBV
601 infection and lytic cycle in NPC cells. Given the involvement of RPL22[45] and RPL4[46], both
602 of which belong to the same RPL family as RPL14[47], in EBV infection, these findings highlight
603 the crucial role of RPL family members in EBV life cycle. Furthermore, our study revealed
604 that *RPL14* inhibits NPC tumorigenesis, consistent with its tumor-suppressive function
605 reported in an *in vitro* NPC study[48] and in other cancer types[49]. Reinforcing this, a high *RPL14*
606 expression is associated with a favorable survival of NPC. Taken together, our findings suggest
607 that the polymorphism at rs2276868 predisposes individuals to varied *RPL14* expression,
608 which in turn influences EBV-related tumorigenesis in NPC.

609 Besides *RPL14* in our study, multiple NPC-associated genes such as *HLA-I, -II*, and *CIITA*
610 have been implicated in modulating EBV life cycle [29,30]. This reinforces that genetic variations
611 affect EBV to mediate varied susceptibility to NPC. Significantly, our findings reveals that the
612 effectiveness of the NPC polygenic risk score is influenced by the serological status of EBV
613 activation. Given that both the EBV DNA load and antibodies against EBV are established
614 serological markers for early NPC diagnosis[60,61], incorporating the rcPRS and EBV infection

615 markers could significantly enhance personalized risk assessments and lead to the development
616 of more effective screening strategies for NPC.

617 Our study has highlighted *SELE* as a novel NPC-associated gene. This association is likely
618 attributed to the rare germline mutation rs5361 in *SELE*, which encodes an adhesion protein E-
619 Selectin, known for its interactions with various cells, including leukocytes and malignant
620 epithelial cells[36,50]. A previous study has demonstrated that the deleterious S149R encoded by
621 rs5361 enhances the functionality of E-Selectin in endothelial cells, promoting their rolling and
622 adhesion capabilities[37]. Noteworthily, our study extends these findings by demonstrating that
623 *SELE* expression is confined to endothelial cells in tumor tissues. Our structural modelling and
624 functional experiments reveal that S149R mutation extends the SELE's side chain on the
625 surface of endothelial cells, thereby augmenting their migration and angiogenesis abilities.
626 Furthermore, we observed that endothelial cells expressing SELE, particularly those with the
627 S149R mutation, significantly render stronger migration and tumorigenesis to malignant NPC
628 cells. This supports the crucial role of E-selectin in interacting with cancer cells and modulating
629 metastasis across various cancers[36,51-53]. Therefore, these findings suggest that the *SELE*-
630 S149R may enhance the adhesion function of E-Selectin in endothelial cells, reshaping the key
631 TME component to favor the progression of cancer cells[53], consequently altering individual
632 susceptibility to NPC.

633 We further delved deeper into the cellular expression of various NPC-associated genes,
634 revealing versatile patterns. For example, certain genes, like *RPL14*, are expressed in most cell
635 types, including epithelial cells that give rise to malignant NPC cells. In contrast, genes like
636 *HLA-II* are found mainly in diverse stromal cells, which typically lack malignant potential in
637 NPC. Such patterns are also observed in other cancers. For instance, the well-known
638 susceptibility-associated genes *NOTCH4* in lung cancer and *SMAD1* in colorectal cancer[54,55]
639 are exclusively expressed in endothelial cells (not typically developing into malignancy) in
640 tumors. These findings highlight the multifaceted cellular implications of germline variations
641 in cancer susceptibility, resonating with a growing literature suggesting the engagement of
642 various cell types in the development of complex disease[56-58]. Given that the validation of the
643 functional relevance of genetic susceptibility genes often predominantly emphasizes the cells
644 of cancer origin (e.g., epithelial cells in NPC), our findings call attention to the importance of
645 exploring the roles of cancer risk genes across diverse TME cell types in cancer development
646 (such as endothelial cells)[54,55].

In summary, our study fills the missing heritability of NPC and enhances our understanding of the genetic architecture of NPC by unveiling novel genetic associations from variants of both common and rare prevalence. Furthermore, our study elucidates diverse pathogenic mechanisms, including the EBV-mediated tumorigenesis in malignant epithelial cells through *RPL14* and the adhesion component in endothelial cells via *SELE*. These findings highlight the substantial impacts of genetic variants on EBV life cycle and various cell types within the TME, which jointly contribute to NPC development. Moreover, our innovative rcPRS model, incorporating these novel discoveries, reflects the modifier effect of EBV status on polygenic risk and provides promising implications for NPC screening. Additionally, we acknowledge limitations, including sample size constraints, especially for the FHNPC group and rarer variants, and the need for further studies to delve into the mechanistic links between these genetic variants and NPC pathogenesis. Future work should explore the potential clinical benefits of these findings in NPC management.

Acknowledgement

We acknowledge supports from the National Natural Science Foundation of China (NSFC; 82261160657, 81971270), the National Key R&D Program of China (NKRDPC; 2022YFC3400901 and 2021ZD0202000), the Sci-Tech Project Foundation of Guangzhou City (201707020039), the Guangdong Innovative and Entrepreneurial Research Team Program (2016ZT06S638), the Chang Jiang Scholars Program (J.X.B.), Hong Kong Research Grant Council (RGC) Theme-based Research Scheme Funds (T12-703/22-R and T12-703/23-N), National Medical Research Council Singapore Clinician Scientist Award (NMRC/CSAINV20nov-0021), the Duke-NUS Oncology Academic Program Goh Foundation Proton Research Programme (M.L.C), NCCS Cancer Fund (M.L.C), the Kua Hong Pak Head and Neck Cancer Research Programme (M.L.C), the Research Grants Council Area of Excellence (AoE) Hong Kong NPC Research (AoE/M-06/08), and the Hong Kong Cancer Fund (M.L.L.). We thank all participants in the study, staffs at the biobank of SYSUCC for sample preparation, staffs at the Tissue Bank for providing NPC blood samples and the patient demographics of the HK cohort, Tan Kah Min's support for technical support and sample processing in SG cohort, and staffs at the High-Throughput Analysis Platform (HTAP) of SYSUCC for data generation and processing.

679

680 **Author contributions**

681 Designed the study: J.X.B, Y.X.Z; procured financial support: J.X.B, M.L.C, M.L.L, M.J;
682 sample recruitment, preparation, and data collection: M.J, F.G.L, C.C.K, Z.L, M.L.L, J.M.K,
683 M.L.C, E.H.O, Y.M.G, J.R.C, S.H, S.Q.L, X.X.C, X.Y, B.W, Y.H.Z, A.Y.X, P.P.W, Q.Y.C,
684 L.Q.T, W.H.J, H.Q.M; analyzed and interpreted data: Y.Z, J.X.B, C.L.L, G.W.L, X.B, Y.L,
685 S.H, Z.H.R, Y.L.C, C.C.K, J.J.L, M.L.C, J.M.K, E.H.O, J.D.M, D.X.L; performed functional
686 experiments: C.L.L, J.X.J, W.X.Y, Y.Q.Z; wrote the paper (original draft): Y.Z, C.L.L, J.X.B;
687 all authors approved the final report.

688

689 **Availability of data and materials**

690 Key data were deposited in the Research Data Deposit public platform (RDD;
691 http://www.researchdata.org.cn).

692

693 **Declaration of interests**

694 The authors declare no competing interests.

695

696 **Materials and Methods**

697 **Ethics**

698 The study was approved by the Sun Yat-sen University Cancer Center (SYSUCC) Ethics
699 Committee (reference no. SL-B2021-032-03), the SingHealth Institutional Review Board (IRB
700 protocol no. 2019/2177), and the Institutional Review Board (IRB) of the University of Hong
701 Kong. Informed consent was obtained from all participants.

702

703 **Patient recruitment and sample preparation**

704 ***Discovery stage***

705 A total of 3,039 NPC patients of Chinese Han ancestry was recruited from Guangzhou in
706 Guangdong province of China (GD-SYSUCC; n= 2,196) by SYSUCC and from Singapore
707 (SG; n=843) by the National Cancer Center (Singapore, collected from 1987-2018). A total of
708 2,692 healthy individuals of Chinese Han ancestry was recruited as controls from local
709 community in Guangdong (GD-SYSUCC; n=1,355) and from Singapore (SG; n =1,337) by

710 Genome Institute of Singapore (Singapore, details have been described previously[63]). All NPC
711 cases were histologically diagnosed. All healthy controls declared free of cancer through
712 questionnaires. After stringent quality control, the discovery dataset consisted of 2,694 NPC
713 cases (2,125 from GD-SYSUCC and 569 from SG) and 2,328 healthy controls (1,068 from
714 GD-SYSUCC and 1,260 from SG). Serum immunoglobulin A (IgA) antibodies to Epstein-Barr
715 virus (EBV) capsid antigen (IgA-VCA) were available for 1,646 NPC patients and 918 controls
716 in GD-SYSUCC subset. Individuals with IgA-VCA >=1:20 was categorized as EBV positive.

717

718 ***Replication stage***

719 The replication dataset included two cohorts: a Zhongshan cohort (GD-ZS) consisting of 1,941
720 cases and 2,265 controls recruited from the Zhongshan city in the Guangdong province by
721 Zhongshan City People's Hospital, and a Hong Kong cohort (HK) consisting of 2,334 cases
722 and 2,507 controls recruited from Hong Kong by the University of Hong Kong. Specifically
723 for the HK cohort, NPC cases and controls were collected by the Tissue Bank established under
724 the Area of Excellence (AoE) program from five Hong Kong public hospitals including Queen
725 Mary Hospital (QMH), Queen Elizabeth Hospital (QEH), Tuen Mun Hospital (TMH), Pamela
726 Youde Nethersole Eastern Hospital (PYNEH), and Princess Margaret Hospital (PMH) from
727 2010 to 2017, details have been described previously[11]. NPC cases were confirmed by
728 histopathology and enrolled with routine staging procedures according to the American Joint
729 Committee on Cancer (AJCC) TNM system, physical examination, and imaging tests. The
730 control population was recruited from the Red Cross and hospital cancer-free individuals from
731 QMH, QEH, TMH, PYNEH, and PMH. We considered GD-ZS as a Guangdong indigenous
732 cohort that shared regional demographic features with the discovery GD-SYSUCC cohort
733 collected from the same province, whereas the HK cohort shared ancestral genetics with other
734 cohorts but was relatively demographically different.

735

736 ***Bulk RNA-Seq samples***

737 Tumor biopsy samples from 93 NPC patients were collected for bulk RNA-seq (labelled as
738 "the Bei-lab collection"), 87 of which had prognosis data available. Additional bulk RNA-seq
739 data of tumor tissues from 113 independent NPC patients with prognosis data available were
740 collected from a published study (labelled as "the Zhang-lab collection")[64]. We further
741 collected nasopharynx samples from 10 cancer-free individuals with inflammations in

742 nasopharynx at SYSUCC, which were used as controls. Biopsies were collected before any
743 treatment and immersed in RNAlater.

744

745 ***NPC samples for Single-cell RNA-seq***

746 Tumor biopsies of 10 NPC patients were collected for single cell RNA sequencing (scRNA-
747 seq) in our previous study[32]. Among them, eight had tumor epithelial cells successfully
748 captured. By extracting data from four additional studies[33,65-67], we further collected scRNA-
749 seq data of 46 NPC tumor samples, 27 of which captured tumor epithelial cells[33,65-67]. In total,
750 scRNA-seq datasets consisting of 56 samples (of which 35 have epithelial cells captured) were
751 used in downstream analyses.

752

753 **Data generation, quality control and annotation**

754 ***Whole exome sequencing and variant calling***

755 Whole blood DNA sample was extracted from all participants in the discovery dataset for
756 whole exome sequencing. Library was constructed using one of the three products: Agilent
757 SureSelect Human All Exon V6+UTR kit, Agilent SureSelect Human All Exon V5+UTR kit,
758 and Roche SeqCap EZ Exome + UTR Target Enrichment Kit. This was followed by sequencing
759 using a paired-end 2 x 150 bp protocol on an Illumina HiSeq instrument. A custom optimized
760 version of Sentieon[68] was applied to preprocess sequencings reads, align reads to human
761 genome using GRCh37 (hg19) assembly as reference, and conduct single nucleotide variant
762 (SNV) calling using algorithms following the GATK best-practice pipeline[69,70]. After GATK's
763 VQSR quality control, hard filtering was applied to remove the variants with 1) Read depth
764 (DP) <10; 2) Allelic Balance (AB) > 0.8 or < 0.2 for heterozygous genotype; 3) Genotype
765 quality (GQ) < 30. For rare variants (minor allele frequency < 0.01), we applied additional
766 stringent quality control based on per-read mutation rate, allelic balance, and strand bias
767 (defined as proportion of allele called by reads from one strand over that by any of the two
768 strands). We used 1000 genome phase 1 high confident SNP set as golden set to establish
769 parameter threshold range where high liability variants can be called. This led to the following
770 filtering for rare variants: 1) refining alignment by removing any read with a mismatch distance
771 against the reference larger than 8 bp (any indel event counts for 1 bp) and re-apply hard
772 filtering as described above; 2) setting variant-sample elements with strand bias > 0.95 or <
773 0.05 for heterozygous genotype, or >0.97 or <0.03 for homozygous genotype to missing; 3)

774 setting variant-sample elements with allelic Balance (AB) > 0.75 or < 0.22 for heterozygous
775 genotype , or with allelic Balance (AB) < 0.95 and > 0.04 for homozygous genotype to missing.

776

777 ***Additional quality control for association test***

778 For both common and rare variants, we further removed variants that are 1) with a missing
779 rate >= 0.02; 2) with a Hardy-Weinberg equilibrium P value <= 1 x 10^{-6} in healthy controls; 3)
780 with a significant differential missing rate between case vs controls (Bonferroni corrected); 4)
781 variants in super duplicates or low complexity regions. Samples were removed if they are 1)
782 with a missing rate > 0.05; 2) with autosomal heterozygosity deviation outside 3 standard
783 deviations of the mean; 3) genetic outliers through eye check or with any the of top four
784 principal component value located outside 6 standard deviations of the mean. These filtering
785 steps were performed using PLINK[71]. We also removed one of each related pair (remained
786 sample t<0.05) using GCTA[72].

787

788 ***HLA genotyping***

789 High resolution WES-based HLA typing was performed on the bam files using HLAScan
790 (v2.1.3) with default parameters and implemented HLA database[73]. PCR amplification HLA
791 typing was also performed on 135 WES samples to cross-validate the WES-based typing
792 procedures. The concordance of the HLA genotypes was high (> 94%) at four-digit resolution
793 level for most HLA genes, except for HLA-DQA1 and -DPB1 with a relatively lower
794 concordance being observed (> 80%). The HLA amino acid (AA) polymorphism was obtained
795 using HLA AA alignments in IPD-IMGT database[74]. The genotypes of HLA SNPs were
796 inferred by the SNP2HLA software[75].

797

798 ***Capture sequencing for targeted genomic regions***

799 DNA library preparation was performed as described in the NadPrep DNA Library Preparation
800 Kit (#1002222; Nanodigmbio, Nanjing, China) for the MGI sequencing platform on the
801 MGISP-960 automated workstation (MGI Tech Co., Ltd., Shenzhen, China), in accordance
802 with the manufacturers' instructions. Hybridization capture-based target enrichment was
803 performed as described in the NadPrep Hybrid Capture Reagents kit (#1005101; Nanodigmbio)
804 on the MGISP-100 automated workstation (MGI Tech Co., Ltd., Shenzhen, China), in

805 accordance with the manufacturers' instructions. The library distribution was analyzed by
806 Qsep100 (BiOptic Inc, New Taipei City, China) and quantified by Qubit dsDNA HS Assay Kit
807 (Invitrogen, Termo Fisher Scientifc Inc, Waltham, USA). Final libraries were sequenced on
808 MGI DNBSEQ-T7 (MGI Tech Co., Ltd., Shenzhen, China) using a pair-end of 150 bp.

809

810 ***Whole transcriptomic sequencing***

811 For bulk RNA-seq, total RNA was extracted from tissue or cell line using Rneasy Mini Kit
812 (Qiagen), with ribosomal RNAs removed by Ribo-Zero Magnetic kit (Illumina). TruSeq RNA
813 Library Prep Kit (Illumina) was used to construct the library, followed by RNA sequencing.
814 RNA-seq was conducted with a pair-end of 150 bp protocol on an Illumina Hiseq X sequencer.
815 Bowtie was used to map post-Qced reads to human reference genome (hg19) and Htseq was
816 used to quantify reads counts[76,77]. Per-gene expression level was normalized using transcripts
817 per million (TPM). scRNA-seq was performed following the manufacturers' instructions (10x
818 Genomics single-cell 5' sequencing and 3' sequencing kits). Details were described in previous
819 studies[32,33,65-67].

820

821 ***Variant annotation***

822 ANNOVAR was used to annotate SNV with following categories[78]:
823 1) SNPs in dbSNP150 database.
824 2) Variants in population genetics database: 1000 genome phase 3, exome and genome subset
825 of the Genome Aggregation Database (EXAC, gnomAD).
826 3) within genes in NCBI RefSeq Gene database.
827 4) within genes of pathways in curated canonical pathways, GO Ontology items and oncogenic
828 signature gene sets as downloaded from Molecular Signatures Database v6.2[79].
829 5) variants that have potential functional consequences as they ranked at top 5% of the rank
830 score of CADD (Combined Annotation Dependent Depletion), or DANN (deleterious
831 annotation of genetic variants using neural networks) or fitCons (fitness consequence score) [80-
832 82].
833 6) 'pathogenic' or 'likely pathogenic' variants as annotated in InterVar database (clinical
834 interpretation of missense variants)[83];

835

836 **Statistical analysis**

837 ***Single-variant-based association test***

838 For variants in non-HLA region, SNVs with a MAF >= 0.001 were included in a logistic
839 regression in which NPC disease status was regressed on the genotype of individual SNV. For
840 variants in HLA region, four types of variants were included in analysis: SNVs, four-digits
841 HLA alleles, six-digits HLA alleles, and amino acids. For each variant, two tests were
842 performed for three binary phenotypes: all NPC cases (ALLNPC) vs controls, and NPC cases
843 with family history (FHNPC) vs controls, respectively. Other covariates in the model includes
844 top five genetic principal components and gender. Bonferroni method was applied in multiple
845 testing correction (N=157,024), with significance threshold P value of 3.2×10^{-7}.

846

847 ***Conditional analysis for single-variant-based associations***

848 To test whether the single-variant association from target SNV was independent of the
849 associations of other SNVs, conditional analysis was performed by jointly fitting each of the
850 SNVs to be conditioned as covariate variable in the regression model.

851

852 ***SNV-set-based association analysis 1: gene-based test***

853 The gene boundary was defined by the transcription start and end sites. These was no MAF-
854 based filtering for this analysis (singletons were also included). Apart from testing using all
855 SNVs (SNV type 1), we also performed test that only consider coding-affecting SNVs. For
856 each SNV type, we tested 4 algorithms that are available on the "SKAT" package in R:

857 1) The original SNP-set (Sequence) Kernel Association Test (SKAT)[84].

858 2) The original Burden test[85].

859 3) SKAT for the combined effect of common and rare variants using the sum test as
860 described previously[86].

861 4) Burden test for the combined effect of common and rare variants using the sum test as
862 described previously[86].

863 For each gene tested using each SNV type for each phenotype, the result from the algorithm
864 with the most significant P value was remained. Top ten genetic principal components and

865 gender were included in the model as covariates. Bonferroni method was applied in multiple
866 testing correction (N=22,228), with significance threshold P value of 2.3×10^{-6}.

867

868 ***SNV-set-based association analysis 2: pathway-based test***

869 The pathway information was downloaded from Molecular Signature Database, including
870 curated canonical pathways, GO Ontology items and oncogenic signature gene sets[79]. After
871 annotating SNVs to the pathways, we performed pathway-level association analysis to test
872 cumulative effect from both rare and common variants within a pathway on NPC risk. To avoid
873 false positive results driven by very small or very large gene set, we excluded pathways with a
874 size larger than 200 genes or smaller than 5 genes. The same grouping and algorithms applied
875 in the gene-based test were also applied here. Multiple testing correction was performed using
876 the FDR method ($N_{pathway}$=6,204).

877

878 ***Meta-analysis for single-variant-based and gene-based associations.***

879 The random effect model (REML) was applied to meta-analyze the association between
880 individual variants and NPC using the R package "metafor"[87]. The summation of logits
881 method[88] was applied to meta-analyze the association between individual genes and NPC using
882 the R package "metap"[89].

883

884 ***Structural modelling of E-selectin***

885 The molecular structure of the E-selectin complexed with glycomimetic antagonist 2-
886 acetamido-2-deoxy-beta-D-glucopyranose (PDB code 4C16) was modelled as previously
887 described[90]. PyMOL with the Adaptive Poisson-Boltzmann Solver plugin was used in the
888 evaluation of the electrostatic surface and the visualization.

889

890 ***Assessing cell-type specific gene expression of NPC and other cancer-associated genes using***
891 ***scRNA-seq data of tumor and non-tumor tissues***

892 Susceptibility gene list of NPC, lung, colorectal and gastric cancers included those identified
893 in present study (for NPC only) and those collected from published GWAS studies (**Table S10)**.
894 Expression profiles were derived from multiple scRNA-seq datasets: the NPC tumor dataset

895 (n_{sample}=56, n_{cell}= 223,593) as described in "NPC samples for Single-cell RNA-seq" section;
896 the lung cancer tumor dataset (n_{sample}=19, n_{cell}=90,477) downloaded from the GEO database
897 (GSE131907, GSE139555) and collected from a previous pan-cancer study[91]; the gastric
898 cancer tumor dataset (n_{sample}=9, n_{cell}=28,299) provided by a published study[92]; the colorectal
899 cancer tumor dataset (n_{sample}=37, n_{cell}=70,015) downloaded from the GEO database
900 (GSE132465, GSE144735 and GSE139555); and the non-cancer tissue dataset consisting of
901 483,152 cells (for computational consideration, 100,000 cells were randomly selected in
902 downstream analyses) from 10 tissues of 15 donors provided by a published study[37]. The
903 quantification of gene expression and determination of cell types were performed separately
904 for each dataset.

905 Specifically, for NPC data we first used DoubletFinder to detect doublets[93] by inspecting
906 abnormal clusters that simultaneously express two or more cell type markers. For each sample,
907 doublets were removed with the expected doublet rate of 0.05. Cells with $n_{Feature_RNA} > 500$,
908 $n_{Count_RNA} > 1{,}000$ and percent.mt < 25% were retained for downstream analyses. Expression
909 Matrix of all cells were converted to a Seurat object and managed by Seurat's pipeline[94]:
910 normalization with NormalizeData and ScaleData, batch effect correction with Harmony[95],
911 dimensionality reduction with RunUMAP, clustering with FindNeighbors (k.param = 30) and
912 FindClusters. Clusters were annotated by classic markers as following: NK cells (KLRF1), T
913 cells (CD3D), Plasma cells (MZB1), B cells (MS4A1), Myeloid cells (AIF1), Cancer
914 Associated Fibroblasts (COL1A1), Endothelial cells (VWF) and Epithelial cells (EPCAM).
915 Normalized expression of marker genes for each cell type in each tumor datasets were shown
916 in **Figure S12**.

917 Lung, gastric, colorectal cancer tissue datasets were merged and analyzed. We first used
918 Scrublet[96] to remove estimated doublets and SoupX[97] to remove cell-free mRNA
919 contamination. Cells with $n_{Feature_RNA} > 500$, $n_{Count_RNA} > 1000$ and percent.mt < 25% through
920 quality control were kept for downstream analysis. NormalizeData and ScaleData in Seurat
921 was used to normalize data[98]; FindVariableFeatures with $n_{feature}$ = 3000 was used to select
922 hypervariable genes. We used Harmony to correct for batch effect caused by different patients[95],
923 and used RunUMAP with dims = 1:30 and FindClusters with resolution = 0.3 for dimension
924 reduction and clustering. The clusters were annotated by classic markers of major cell types.
925 Normalized expression of marker genes for each cell type in each tumor datasets were shown
926 in **Figure S12**.

927 For the non-cancer tissue dataset, cell clusters were determined by the original study[37].

928

929 ***Inference of malignant status of epithelial cells in scRNA-seq data in NPC tumor tissues***

930 Malignant cells have substantially increased copy number variation (CNV), such as large-scale
931 gain or deletions of chromatin. Therefore, we use inferCNV to identify malignant epithelial
932 cell clusters[99]. Comparing with control normal epithelial cells downloaded from GEO database
933 (GSE121600), all epithelial cell clusters identified in NPC scRNA-seq data in our study were
934 considered malignant.

935

936 ***Estimate of WES-SNV heritability for NPC***

937 GREML-LDMS (the LD and MAF stratified GREML) approach was applied to estimate the
938 proportion of NPC risk that can be explained by WES SNVs [100]. In brief, when calculating the
939 total WES SNV-heritability and the proportion explained by variants from HLA and non-HLA
940 regions, SNVs were stratified into four groups based on MAF and regions: MAF ≥ 0.01 in
941 HLA region, MAF<0.01 HLA region, MAF ≥ 0.01 in non-HLA region and MAF < 0.01 in
942 non-HLA region; when further decomposing the WES SNV-heritability in non-HLA region,
943 SNVs were stratified into 28 groups based on LD scores (four bins based on quartiles. LD score
944 was calculated as the sum of R^2 with variants in a 200kb window) and MAF (7 bins: 0.0005 <
945 MAF <= 0.001 ,0.001 < MAF <=0.01, 0.01 < MAF <=0.1, 0.1 < MAF <= 0.2, 0.2 < MAF
946 <=0.3, 0.3 < MAF <=0.4, and 0.4 < MAF <=0.5). For each SNV group, genomic relationship
947 matrix (GRM) was created. In each model (the four components and 28 components ones),
948 GRMs from all groups were then simultaneously fitted in the GREML model for NPC, where
949 the total NPC variation explained by all genetic components and the variation explained by
950 individual genetic component as represented by each GRM can by estimated.

951

952 ***Joint model for a comparative analysis to estimate the relative risks by RPL14, SELE, HLA,***
953 ***and non-HLA GWAS loci***

954 In discovery samples, a subset (1,382 cases and 912 controls) of the GD-SYSUCC cohort
955 simultaneously have imputed GWAS array[17] and WES data available, allowing the
956 comparisons of the relative disease risks conferred by the common variant rs2276868 in *RPL14*
957 and the rare variant *rs5361* in SELE with the polygenic risk from the HLA and other known
958 GWAS loci. In replication samples, the cap-seq designed to target at both published GWAS

959 loci and the candidate loci identified by the presented WES study also enabled this comparison.
960 In brief, for each cohort we applied a joint regression model that simultaneously accounts for
961 genetic effects from different variants: the effects from *RPL14* and *SELE* were presented by
962 the genotypes of rs2276868 (*RPL14*) and rs5361(*SELE*), respectively; the combined genetic
963 effects from published non-HLA GWAS loci and that from HLA loci were represented as two
964 polygenic risk scores (one for non-HLA GWAS loci and one for HLA loci) constructed using
965 odds ratios estimated from original publication or our single-variant analysis using discovery
966 cohorts (**Table S14**).

967

968 ***Construction and evaluation of polygenic risk scores (PRS) for NPC***

969 ***1. Construction of a refined composite PRS (rcPRS) for NPC risk***

970 The rcPRS was calculated for all individuals with non-missing genotypes in the discovery
971 sample (the subset of 1,382 cases and 912 controls with both GWAS array and WES data
972 available[17] in GD-SYSUCC cohort) and in all replication samples (the capture sequencing
973 allowed the genotyping for constituent variants of combined PRS). The following SNVs were
974 used to create rcPRS to simultaneously account for genetic risk factors identified in our WES
975 analyses and published GWASs[8,17,101]:

976 1) In WES data, significant variants in single-variant-based association test (including HLA
977 variants identified in conditional analysis).
978 2) In WES data, leading variants in gene-based test if they:
979 a. were in genes significant in SKAT-gene-based association test.
980 b. reached $P<1\times10^{-4}$ in single-SNV-based association test.
981 3) In WES data, leading variants in pathway-based test as they:
982 a. were in a gene of significant pathways and that gene has a $P<0.01$ in gene-based test.
983 b. reached $P<1\times10^{-4}$ in single-SNV-based association test.
984 4) Published GWAS loci [8,17,101]. Only non-HLA GWAS loci was extracted from this source
985 as majority of HLA SNPs identified in published GWAS were in non-coding regions,
986 which are beyond the regions captured by WES and that signals from HLA regions have
987 already been included in source 1.

988 To avoid duplication due to overlapped genes among pathways, each variant can be used
989 only once. Clumping was performed so that in each cluster of LD partners with $R^2>=0.1$ (within
990 250kb extended windows) only one variant could be remained. PRS was created as the sum of

991 weighted genetic risk from all variants. For each variant, the weighted genetic risk was
992 calculated as the product of allele dosage and the coefficient of variant effect estimated in
993 single-variant-based test. For variants from published GWAS, the coefficient was extracted
994 from original publications [8,17,101]. Details of the constituent variants were shown in **Table S15**.

995

996 ***2. Construction of GWAS-only PRS (gPRS) for NPC risk***

997 For a subset sample (n=2, 294) of the discovery GD-SYSUCC cohort, we produced imputed
998 genotypes for BeadChips array data. In brief, SNP array data was obtained from a previous
999 study[8]. To prepare the data for imputation analysis, we first used Liftover to convert the SNP
1000 array data from hg18 to hg19 encoding strand. Next, we performed quality control at the SNP
1001 level, removing SNPs with a minor allele frequency (MAF) less than 0.01, genotype missing
1002 rate greater than 0.05, and those that failed the Hardy-Weinberg equilibrium test (HWE) with
1003 a P-value less than 10^{-5}. A total of 463,270 SNPs passed quality control and were retained for
1004 further analysis. For the quality-controlled genotype data, we used SHAPEIT2 with default
1005 parameters to estimate haplotypes of the study samples[102]. We then used IMPUTE2 with
1006 default parameters and the haplotype data from the 1000 Genomes Project to impute the
1007 missing genotype of each individual's haplotype[103]. After imputation, we removed SNPs with
1008 an INFO value less than 0.8 and set loci with genotype probability (GP) values less than 0.9 to
1009 missing. Ultimately, we retained 6,095,964 SNPs for analysis. This allows the construction of
1010 a previous published PRS using NPC-associated loci reported by GWAS[10], following the
1011 instruction from the original study[10]. To note, for three SNPs (rs2106123, rs6475604,
1012 rs9507124) not genotyped and not imputed in GD-SYSUCC, we used three surrogate SNPs in
1013 complete LD (R^2=1 in Chinese Southern Han population in 1000 genome phase 3 dataset) with
1014 them (rs6774494 for rs2106123, rs1412829 for rs6475604, and rs9510790 for rs9507124) in
1015 the model.

1016

1017 ***Construction of composite scores for pathway and EBV activity***

1018 We applied the AddModuleScore function in R package Seurat [98] to profile each pathway from
1019 the REACTOME and the GO Ontology database in each sample, where bulk RNA-seq or
1020 scRNA-seq data was available. Based on AddModuleScore, the pathway score is obtained by
1021 subtracting the average expression of the corresponding control gene set from the average
1022 expression of the target gene set. For samples with scRNA-seq, we took each patient as a

1023 datapoint, meaning that the average expression of a given gene across all epithelial cells from
1024 the patient was treated as the expression of that gene for the patient. We additionally created
1025 composite scores for EBV activity. In brief, we downloaded the EBV gene list from the EBV
1026 reference sequence (Akata; https://github.com/flemingtonlab/public/tree/master/annotation)
1027 and mapped the scRNA-seq data of EBV-positive malignant epithelial cells onto them. We
1028 then used the annotated EBV gene data to construct an EBV-composite score for each NPC
1029 patient with scRNA-seq data derived from EBV-positive epithelial cells available, following
1030 the same steps as described above.

1031

1032 ***The correlation between the pathway composite scores and RPL14 expression***

1033 Pearson correlations between *RPL14* expression and composite scores were tested using the
1034 cor.test function in R. Multiple testing correction was performed using the FDR method. The
1035 Pearson correlations of individual EBV genes and *RPL14* were shown in **Table S17.**

1036

1037 **Functional characterization of NPC-associated loci**

1038 ***Cell culture***

1039 Human NPC cell lines S26, CNE2-EBV, and HONE1-EBV were kindly gifted by Professor
1040 Mu-Sheng Zeng at the SYSUCC. Human NPC cell lines HK-1 and C666-1 were kindly gifted
1041 by Professor KW Lo at the Chinese University of Hong Kong. Human embryonic kidney cell
1042 293T cell was purchased from Cell Bank of Type Culture Collection of Chinese Academy of
1043 Sciences, Chinese Academy of Sciences. All above cells were cultivated in DMEM medium
1044 containing 10% fetal bovine serum (FBS, Gibco, NY, USA) and 1% penicillin–streptomycin
1045 solution (FBS, Gibco, NY, USA). Human umbilical vein endothelial cells (HUVECs) were
1046 isolated and cultured in ECM medium (ScienCell, CA, USA) supplemented with 15% FBS and
1047 0.03 mg/mL of endothelial cell growth supplement (ECGS, ScienCell, CA, USA). All cells
1048 were cultured at 37°C under a humidified atmosphere with 5% CO2. For all cell lines,
1049 mycoplasma was routinely determined using PCR with specific primers and no contamination
1050 was detected (**Table S18**).

1051

1052 ***Cell proliferation***

1053 For cell growth curves, a total of 1×10^5 NPC cells was plated in a 12-well plate with three
1054 replicates. The number of cells was measured by a cell counter with trypan blue staining on 24,
1055 48 and 72h. For colony formation assays, NPC cells were seeded at a density of 3000 cells per
1056 replicate into 6-well plate for 7-10 days. Then, colonies were fixed with 4% paraformaldehyde
1057 for 30min at room temperature. After stained with crystal violet for 10min, cells were
1058 photographed with the Bio-Rad ChemiDoc Touch (Hercules, CA, USA).

1059

1060 ***Cell migration***

1061 Transwell assay was performed as described previously[104]. Briefly, NPC cells in serum-free
1062 medium were plated at a density of 6×10^4 cells into the transwell chamber (8 μm pores, Corning,
1063 NY, USA), which then placed at 24-well plates containing 600 μL DMEM suppled with 10%
1064 FBS. After 16-24h, cells on the membrane were fixed with 4% paraformaldehyde for 30min
1065 and stained with trypan blue solution for 15min at room temperature. Then the cells were
1066 imaged under a microscope.

1067

1068 ***Luciferase reporter assay***

1069 Luciferase reporter assay was performed as described previously[105]. Briefly, the promoter
1070 region of RPL14 containing the rs2276868-C or -T was cloned into a luciferase reporter pGL3-
1071 basic plasmid. Afterwards, 293T cells were co-transfected with 200 ng of pGL3-RPL14-C or
1072 -T constructs and 10 ng of pRL (Renilla luciferase) plasmid together with respective siRNAs
1073 or overexpression plasmids. After 48h, cells were harvested to measure the luciferase activity
1074 through a Dual-Luciferase Assay Kit (Promega, USA) according to the manufacturer's
1075 instructions.

1076

1077 ***Immunofluorescence staining (IF) and immunohistochemistry (IHC)***

1078 Paraffin slides of xenograft tumors were deparaffinized with xylene and rehydrated through a
1079 gradient ethanol series. After microwave antigen retrieval in sodium citrate solution (pH 6),
1080 slides were incubated in 0.3% hydrogen peroxide for 15 min at room temperature to quench
1081 the endogenous peroxidase activity. Afterwards, the samples were incubated with the primary
1082 anti-Ki-67 (AB_393778, BD Pharmingen™, USA) or CD34 (GB13013, Servicebio, China)
1083 antibodies overnight at 4 °C. Next day, for IF, Alexa Fluor-conjugated secondary antibody

1084 (Thermo Fisher Scientific, USA) was used for 1 h at room temperature, followed by
1085 counterstaining with antifade mounting medium and 4′ ,6-diamidino-2-phenylindole (DAPI)
1086 for 10 min. Images were then captured with a confocal laser scanning microscope (Carl Zeiss,
1087 Microscope 880, Germany). For IHC, after exposure to secondary antibodies at room
1088 temperature for 1h, chromogenic detection was performed using 0.05% 3,30-diaminobenzidine
1089 (Dako, Denmark). Hematoxylin was applied for counterstaining. Two independent
1090 pathologists from SYSUCC evaluated staining intensity. Afterwards, IHC scores were then
1091 calculated, combining staining intensity and the proportion of stained cells.

1092

1093 ***Manipulating gene expression using siRNA and lentivirus***

1094 For transient knockdown of target genes, siRNAs specific against RPL14 or NKRF were
1095 transfected into cells using Lipofectamine RNAiMAX (Invitrogen, USA) according to the
1096 manufacturer's protocol. After 48-72 hours, cells were harvested to detect the knockdown
1097 efficiency of target genes through RT-qPCR as described below. Full length cDNA of NKRF
1098 was cloned into the pcDNA3.1 vectors. RPL14, SELE-WT and MUT were cloned into the
1099 pCDH-puro lentiviral vectors. For lentivirus preparation, 293T cells were transfected with
1100 above lentivirus plasmids or control vector using Lipofectamine 2000 (Invitrogen, USA)
1101 according to the manufacture's procedures. Afterwards, the supernatant media containing
1102 lentivirus were collected two times at 24 and 48h post-transfection to infect NPC cell lines,
1103 following selection with puromycin (2 μg/mL) at least for one week.

1104

1105 ***RNA isolation, RT-qPCR and ChIP PCR***

1106 Total RNA was isolated using Trizol reagent (Invitrogen, USA) following the manufacturer's
1107 protocols. After determination of RNA concentration using a Nanodrop Spectrophotometer
1108 (Thermo Fisher Scientific, USA), cDNA was synthesized using oligo (dT) primers and M-
1109 MLV Reverse Transcriptase (Promega, USA) according to the manufacturer's procedures. RT-
1110 qPCR was performed with SYBR Premix Ex Taq kit (Takara, Japan) on a LightCycler 96 (Bio-
1111 rad, USA). GAPDH or 18S RNA was used as an internal control. The primer sequences are
1112 shown in **Table S18**. For ChIP assay, S26 cells transfected with Flag-NKRF plasmids or
1113 control vectors were grown in complete DMEM media to 80%–90% confluency. The media
1114 were removed and replaced with media containing 1% formaldehyde and crosslinked for
1115 10 min at 37°C, followed by SimpleChIP® Plus Enzymatic Chromatin IP Kit (Magnetic Beads;

1116 CST, USA) according to the manufacturer's instructions. Afterwards, PCR or qPCR was
1117 performed with specific detection primers following the standard procedures (**Table S18**).

1118

1119 ***EBV preparation and infection***

1120 AKATA cells carrying EBV recombinant viruses were treated with 0.75 (v/v) of goat anti-
1121 human immunoglobulin G IgG (H0111-6, Tianfun Xinqu Zhenglong Biochem, China) for 6h
1122 at 37℃ to induce the viral productive cycle. Virus supernatants were harvested three days post-
1123 induction, filtered through a 0.45 μm filter and concentrated at 20000g for 3h. Afterwards,
1124 virus concentrate was added into NPC cells and concentrated at 2000g in 37℃ for 1h. Cell
1125 supernatants were removed and replaced with normal media 6-8h post-infection. The infection
1126 efficiency was measured using flow cytometry analysis of GFP-positive cells.

1127

1128 ***Western blotting***

1129 NPC cells were lysed in ice-cold cell lysis buffer (CST, USA) containing 1X protease inhibitors
1130 (Beyotime, China). Lysate was cleared by centrifugation at 14,000g for 10 min at 4°C and
1131 boiled in 1X LDS loading buffer at 100°C for 10 min. Proteins were separated by SDS-PAGE
1132 and transferred to 0.2 μm polyvinylidene difluoride (PVDF) membrane (Merck Millipore,
1133 USA). Membranes were blocked with 5% bovine serum albumin (BSA; Sangon Biotech, China)
1134 in tris-buffered saline and Tween 20 (TBST) at room temperature for 1h. Afterwards, the
1135 membranes were incubated with target-specific antibodies in blocking buffer at 4°C overnight.
1136 Next day, horseradish peroxidase–conjugated (HRP) secondary antibodies were used at room
1137 temperature for 1h. Proteins were then detected with Fdbio-Dura ECL kit (Fdbio science, China)
1138 and quantified by Bio-Rad ChemiDoc Touch (Hercules, USA). Primary antibodies were
1139 commercially available, including RPL14 and LMP1 (ab181200 and ab78113, Abcam, USA),
1140 SELE (20894-1-AP, Proteintech, China), Flag (F1804, Sigma-Aldrich, USA), BZLF1(sc53904,
1141 Santa Cruz, USA) and ACTIN (AC004, Abclonal, China).

1142

1143 ***In vivo tumor xenograft***

1144 Six-week-old male BALB/c nude mice (Beijing Vital River Laboratory Animal Technology,
1145 China) were grown in the Specific Pathogen Free (SPF) environment. For subcutaneous
1146 xenograft assay, 5×10^6 CNE2-EBV cells or 2×10^6 S26 cells co-culturing with HUVEC cells

1147 (S26: HUVEC = 10:1) were suspended in 100μL ice-old PBS mixed with Matrigel (0.20 v/v,
1148 Corning Incorporated, USA) and subcutaneously injected to the two flanks of the mice.
1149 Macroscopic observation and tumor volume measurement using a caliper were performed
1150 every 3 days. After 15 days, all mice were sacrificed, and tumor tissues were carefully dissected
1151 and weighed. Tumor volume was calculated following the formula: tumor volume (mm3) =
1152 length (mm) × (width (mm)) 2 /2. For tumor lymphatic metastasis assay, 1×10^6 S26 cells co-
1153 culturing with HUVEC cells (S26: HUVEC = 10:1) were injected into the foot pads of the node
1154 mice. After one month, the lymph nodes were harvested, volumed and paraffin embedded
1155 further HE staining. For animal studies *in vivo*, all experiments were performed in strict
1156 accordance with the instructions approved by the Institutional Animal Care and Use Committee
1157 of Sun Yat-sen University.

1158

1159 ***Tube formation assays***

1160 For tube formation assays, HUVEC cells stably expressing SELE wild-type (SELE-WT), the
1161 S149R mutant or control vectors were resuspended in the ECM medium. Then the cells were
1162 seeded into 96-well plates pre-coated with growth-factor-reduced Matrigel (Corning
1163 Incorporated, USA) and incubated at 37°C for 5 hours. The formation of capillary-like
1164 structures was subsequently observed using a microscope. Quantitative analysis was conducted
1165 by counting the number of tube networks formed across the entire field, serving as an indicator
1166 of *in vitro* angiogenesis capability.

1167

1168 **References**

1169 1 Chen, Y.-P. *et al.* Nasopharyngeal carcinoma. *The Lancet* **394**, 64-80,
1170 doi:10.1016/s0140-6736(19)30956-0 (2019).
1171 2 Wei, K. R. *et al.* Nasopharyngeal carcinoma incidence and mortality in China, 2013.
1172 *Chin J Cancer* **36**, 90, doi:10.1186/s40880-017-0257-9 (2017).
1173 3 Cao, S. M., Simons, M. J. & Qian, C. N. The prevalence and prevention of
1174 nasopharyngeal carcinoma in China. *Chin J Cancer* **30**, 114-119,
1175 doi:10.5732/cjc.010.10377 (2011).
1176 4 Chen, C. *et al.* Multiple risk factors of nasopharyngeal carcinoma: Epstein-Barr virus,
1177 malarial infection, cigarette smoking and familial tendency. **10**, 547-553 (1990).
1178 5 IRELAND, B., LANIER, A. P., KNUTSON, L., CLIFT, S. E. & HARPSTER, A. J. I.
1179 j. o. e. Increased risk of cancer in siblings of Alaskan native patients with
1180 nasopharyngeal carcinoma. **17**, 509-511 (1988).
1181 6 Loh, K. S. *et al.* Familial nasopharyngeal carcinoma in a cohort of 200 patients. **132**,
1182 82-85 (2006).
1183 7 Liu, Z. *et al.* Quantification of familial risk of nasopharyngeal carcinoma in a high-
1184 incidence area. **123**, 2716-2725 (2017).

1185 8 Bei, J. X. *et al.* A genome-wide association study of nasopharyngeal carcinoma
1186 identifies three new susceptibility loci. *Nature genetics* **42**, 599-603,
1187 doi:10.1038/ng.601 (2010).
1188 9 Lu, S.-j. *et al.* Linkage of a nasopharyngeal carcinoma susceptibility locus to the HLA
1189 regions. *Nature* **346**, 470-471 (1990).
1190 10 He, Y. Q. *et al.* A polygenic risk score for nasopharyngeal carcinoma shows potential
1191 for risk stratification and personalized screening. *Nature communications* **13**, 1966,
1192 doi:10.1038/s41467-022-29570-4 (2022).
1193 11 Ning, L. *et al.* Nasopharyngeal carcinoma MHC region deep sequencing identifies
1194 HLA and novel non-HLA TRIM31 and TRIM 39 loci. **3**, 759 (2020).
1195 12 Xiong, W. *et al.* A susceptibility locus at chromosome 3p21 linked to familial
1196 nasopharyngeal carcinoma. **64**, 1972-1974 (2004).
1197 13 Hu, L.-F. *et al.* A genome-wide scan suggests a susceptibility locus on 5p13 for
1198 nasopharyngeal carcinoma. **16**, 343-349 (2008).
1199 14 Fachiroh, J. *et al.* Tobacco consumption and genetic susceptibility to nasopharyngeal
1200 carcinoma (NPC) in Thailand. *Cancer Causes & Control* **23**, 1995-2002,
1201 doi:10.1007/s10552-012-0077-9 (2012).
1202 15 Ng, C. C. *et al.* A genome-wide association study identifies ITGA9 conferring risk of
1203 nasopharyngeal carcinoma. *Journal of human genetics* **54**, 392-397,
1204 doi:10.1038/jhg.2009.49 (2009).
1205 16 Bei, J.-X. *et al.* A GWAS meta-analysis and replication study identifies a novel locus
1206 within CLPTM1L/TERT associated with nasopharyngeal carcinoma in individuals of
1207 Chinese ancestry. **25**, 188-192 (2016).
1208 17 Cui, Q. *et al.* An extended genome-wide association study identifies novel
1209 susceptibility loci for nasopharyngeal carcinoma. **25**, 3626-3634 (2016).
1210 18 Wang, T. M. *et al.* Fine-mapping of HLA class I and class II genes identified two
1211 independent novel variants associated with nasopharyngeal carcinoma susceptibility.
1212 **7**, 6308-6316 (2018).
1213 19 Dai, J. *et al.* Estimation of heritability for nine common cancers using data from
1214 genome-wide association studies in Chinese population. **140**, 329-336 (2017).
1215 20 Huang, S. F. *et al.* Familial aggregation of nasopharyngeal carcinoma in Taiwan. *Oral*
1216 *Oncol* **73**, 10-15, doi:10.1016/j.oraloncology.2017.07.020 (2017).
1217 21 Manolio, T. A. *et al.* Finding the missing heritability of complex diseases. *Nature*
1218 **461**, 747-753, doi:10.1038/nature08494 (2009).
1219 22 Genin, E. Missing heritability of complex diseases: case solved? *Human genetics* **139**,
1220 103-113, doi:10.1007/s00439-019-02034-4 (2020).
1221 23 Dai, W. *et al.* Whole-exome sequencing identifies MST1R as a genetic susceptibility
1222 gene in nasopharyngeal carcinoma. *Proceedings of the National Academy of Sciences*
1223 **113**, 3317-3322, doi:10.1073/pnas.1523436113 (2016).
1224 24 Yu, G. *et al.* Whole-Exome Sequencing of Nasopharyngeal Carcinoma Families
1225 Reveals Novel Variants Potentially Involved in Nasopharyngeal Carcinoma. *Scientific*
1226 *reports* **9**, doi:10.1038/s41598-019-46137-4 (2019).
1227 25 Wang, T. M. *et al.* Whole-Exome Sequencing Study of Familial Nasopharyngeal
1228 Carcinoma and Its Implication for Identifying High-Risk Individuals. *J Natl Cancer*
1229 *Inst* **114**, 1689-1697, doi:10.1093/jnci/djac177 (2022).
1230 26 Xiao, R. W. *et al.* Rare POLN mutations confer risk for familial nasopharyngeal
1231 carcinoma through weakened Epstein-Barr virus lytic replication. *EBioMedicine* **84**,
1232 104267, doi:10.1016/j.ebiom.2022.104267 (2022).
1233 27 Chan, K. A. *et al.* Analysis of plasma Epstein–Barr virus DNA to screen for
1234 nasopharyngeal cancer. **377**, 513-522 (2017).

1235 28 Li, T. *et al.* Anti–Epstein–Barr Virus BNLF2b for Mass Screening for
1236 Nasopharyngeal Cancer. **389**, 808-819 (2023).
1237 29 Winter, J. R. *et al.* Predictors of Epstein-Barr virus serostatus in young people in
1238 England. **19**, 1-9 (2019).
1239 30 Hatton, O. L., Harris-Arnold, A., Schaffert, S., Krams, S. M. & Martinez, O. M. J. I. r.
1240 The interplay between Epstein–Barr virus and B lymphocytes: implications for
1241 infection, immunity, and disease. **58**, 268-276 (2014).
1242 31 Su, Z. Y., Siak, P. Y., Leong, C.-O. & Cheah, S.-C. J. F. i. m. The role of Epstein–
1243 Barr virus in nasopharyngeal carcinoma. **14**, 1116143 (2023).
1244 32 Liu, Y. *et al.* Tumour heterogeneity and intercellular networks of nasopharyngeal
1245 carcinoma at single cell resolution. *Nature communications* **12**, 741,
1246 doi:10.1038/s41467-021-21043-4 (2021).
1247 33 Chen, Y.-P. *et al.* Single-cell transcriptomics reveals regulators underlying immune
1248 cell diversity and immune subtypes associated with prognosis in nasopharyngeal
1249 carcinoma. **30**, 1024-1042 (2020).
1250 34 Altshuler, D. M. *et al.* A global reference for human genetic variation. *Nature* **526**,
1251 68-74, doi:10.1038/nature15393 (2015).
1252 35 Karczewski, K. J. *et al.* The mutational constraint spectrum quantified from variation
1253 in 141,456 humans. *Nature* **581**, 434-443, doi:10.1038/s41586-020-2308-7 (2020).
1254 36 Trinh, C. T. H. *et al.* LMP1-EBV Gene Deletion Mutations and HLA Genotypes of
1255 Nasopharyngeal Cancer Patients in Vietnam. *Pathophysiology* **30**, 1-12,
1256 doi:10.3390/pathophysiology30010001 (2023).
1257 37 Tabula Sapiens, C. *et al.* The Tabula Sapiens: A multiple-organ, single-cell
1258 transcriptomic atlas of humans. *Science* **376**, eabl4896, doi:10.1126/science.abl4896
1259 (2022).
1260 38 Moore, J. E. *et al.* Expanded encyclopaedias of DNA elements in the human and
1261 mouse genomes. **583**, 699-710 (2020).
1262 39 Tsao, S. W., Tsang, C. M. & Lo, K. W. Epstein-Barr virus infection and
1263 nasopharyngeal carcinoma. *Philosophical transactions of the Royal Society of*
1264 *London. Series B, Biological sciences* **372**, doi:10.1098/rstb.2016.0270 (2017).
1265 40 Yasmin-Karim, S., King, M. R., Messing, E. M. & Lee, Y.-F. J. O. E-selectin ligand-1
1266 controls circulating prostate cancer cell rolling/adhesion and metastasis. **5**, 12097
1267 (2014).
1268 41 Yoshida, M. *et al.* E-selectin polymorphism associated with myocardial infarction
1269 causes enhanced leukocyte-endothelial interactions under flow conditions. **23**, 783-
1270 788 (2003).
1271 42 Dornbos, P. *et al.* A combined polygenic score of 21,293 rare and 22 common
1272 variants improves diabetes diagnosis based on hemoglobin A1C levels. *Nature*
1273 *genetics* **54**, 1609-1614, doi:10.1038/s41588-022-01200-1 (2022).
1274 43 Van Den Bogaert, A. *et al.* The DTNBP1 (dysbindin) gene contributes to
1275 schizophrenia, depending on family history of the disease. **73**, 1438-1443 (2003).
1276 44 Coccia, M., Rossi, A., Riccio, A., Trotta, E. & Santoro, M. G. J. P. o. t. N. A. o. S.
1277 Human NF-κB repressing factor acts as a stress-regulated switch for ribosomal RNA
1278 processing and nucleolar homeostasis surveillance. **114**, 1045-1050 (2017).
1279 45 Yi, M. *et al.* Rediscovery of NF-kappaB signaling in nasopharyngeal carcinoma: How
1280 genetic defects of NF-kappaB pathway interplay with EBV in driving oncogenesis? *J*
1281 *Cell Physiol* **233**, 5537-5549, doi:10.1002/jcp.26410 (2018).
1282 46 Elia, A., Vyas, J., Laing, K. G. & Clemens, M. J. J. E. j. o. b. Ribosomal protein L22
1283 inhibits regulation of cellular activities by the Epstein-Barr virus small RNA EBER-1.
1284 **271**, 1895-1905 (2004).

1285 47 Shen, C.-L. *et al.* Ribosome protein L4 is essential for Epstein–Barr virus nuclear
1286 antigen 1 function. **113**, 2229-2234 (2016).
1287 48 Klinge, S., Voigts-Hoffmann, F., Leibundgut, M., Arpagaus, S. & Ban, N. J. S.
1288 Crystal structure of the eukaryotic 60 S ribosomal subunit in complex with initiation
1289 factor 6. **334**, 941-948 (2011).
1290 49 Zhang, Z., Zhang, Y., Qiu, Y., Mo, W. & Yang, Z. J. B. Human/eukaryotic ribosomal
1291 protein L14 (RPL14/eL14) overexpression represses proliferation, migration, invasion
1292 and EMT process in nasopharyngeal carcinoma. **12**, 2175-2186 (2021).
1293 50 Huang, X.-P. *et al.* Alteration of RPL14 in squamous cell carcinomas and
1294 preneoplastic lesions of the esophagus. **366**, 161-168 (2006).
1295 51 Telen, M. J. J. H. O. C. Cellular adhesion and the endothelium: E-selectin, L-selectin,
1296 and pan-selectin inhibitors. **28**, 341-354 (2014).
1297 52 Köhler, S., Ullrich, S., Richter, U. & Schumacher, U. J. B. j. o. c. E-/P-selectins and
1298 colon carcinoma metastasis: first in vivo evidence for their crucial role in a clinically
1299 relevant model of spontaneous metastasis formation in the lung. **102**, 602-609 (2010).
1300 53 Zen, K. *et al.* CD44v4 is a major E-selectin ligand that mediates breast cancer cell
1301 transendothelial migration. **3**, e1826 (2008).
1302 54 Esposito, M. *et al.* Bone vascular niche E-selectin induces mesenchymal–epithelial
1303 transition and Wnt activation in cancer cells to promote bone metastasis. **21**, 627-639
1304 (2019).
1305 55 Zhang, B. *et al.* NOTCH4ΔL12_16 sensitizes lung adenocarcinomas to EGFR-TKIs
1306 through transcriptional down-regulation of HES1. **14**, 3183 (2023).
1307 56 Zhou, J. *et al.* Long noncoding RNA MALAT1 sponging miR-26a-5p to modulate
1308 Smad1 contributes to colorectal cancer progression by regulating autophagy.
1309 *Carcinogenesis* **42**, 1370-1379, doi:10.1093/carcin/bgab069 (2021).
1310 57 Sato, G. *et al.* Pan-cancer and cross-population genome-wide association studies
1311 dissect shared genetic backgrounds underlying carcinogenesis. **14**, 3671 (2023).
1312 58 Ma, Y. *et al.* Integrating single-cell sequencing data with GWAS summary statistics
1313 reveals CD16+ monocytes and memory CD8+ T cells involved in severe COVID-19.
1314 **14**, 16 (2022).
1315 59 Skene, N. G. *et al.* Genetic identification of brain cell types underlying schizophrenia.
1316 **50**, 825-833 (2018).
1317 60 Witte, J. S., Visscher, P. M. & Wray, N. R. The contribution of genetic variants to
1318 disease depends on the ruler. *Nature reviews. Genetics*, doi:10.1038/nrg3786 (2014).
1319 61 Li, Q. & Cohen, J. I. J. C. c. m. r. Epstein-Barr virus and the human leukocyte antigen
1320 complex. **6**, 175-181 (2019).
1321 62 Su, C. *et al.* EBNA2 driven enhancer switching at the CIITA-DEXI locus suppresses
1322 HLA class II gene expression during EBV infection of B-lymphocytes. **17**, e1009834
1323 (2021).
1324 63 Li, Z. *et al.* Association of rare CYP39A1 variants with exfoliation syndrome
1325 involving the anterior chamber of the eye. **325**, 753-764 (2021).
1326 64 Zhang, L. *et al.* Genomic Analysis of Nasopharyngeal Carcinoma Reveals TME-
1327 Based SubtypesGenomic Subtypes of Nasopharyngeal Carcinoma. **15**, 1722-1732
1328 (2017).
1329 65 Jin, S. *et al.* Single-cell transcriptomic analysis defines the interplay between tumor
1330 cells, viral infection, and the microenvironment in nasopharyngeal carcinoma. **30**,
1331 950-965 (2020).
1332 66 Zhao, J. *et al.* Single cell RNA-seq reveals the landscape of tumor and infiltrating
1333 immune cells in nasopharyngeal carcinoma. **477**, 131-143 (2020).

1334 67 Gong, L. *et al.* Comprehensive single-cell sequencing reveals the stromal dynamics
1335 and tumor-specific characteristics in the microenvironment of nasopharyngeal
1336 carcinoma. **12**, 1-18 (2021).
1337 68 Aldana, R. & Freed, D. Data Processing and Germline Variant Calling with the
1338 Sentieon Pipeline. *Methods in molecular biology* **2493**, 1-19, doi:10.1007/978-1-
1339 0716-2293-3_1 (2022).
1340 69 Kendig, K. I. *et al.* Sentieon DNASeq variant calling workflow demonstrates strong
1341 computational performance and accuracy. **10** (2019).
1342 70 DePristo, M. A. *et al.* A framework for variation discovery and genotyping using
1343 next-generation DNA sequencing data. **43**, 491 (2011).
1344 71 Purcell, S. *et al.* PLINK: A tool set for whole-genome association and population-
1345 based linkage analyses. *American journal of human genetics* **81**, 559-575, doi:Doi
1346 10.1086/519795 (2007).
1347 72 Yang, J., Lee, S. H., Goddard, M. E. & Visscher, P. M. GCTA: a tool for genome-
1348 wide complex trait analysis. *American journal of human genetics* **88**, 76-82,
1349 doi:10.1016/j.ajhg.2010.11.011 (2011).
1350 73 Ka, S. *et al.* HLAscan: genotyping of the HLA region using next-generation
1351 sequencing data. **18**, 1-11 (2017).
1352 74 Robinson, J. *et al.* Ipd-imgt/hla database. **48**, D948-D955 (2020).
1353 75 Jia, X. *et al.* Imputing amino acid polymorphisms in human leukocyte antigens. **8**,
1354 e64683 (2013).
1355 76 Langmead, B., Trapnell, C., Pop, M. & Salzberg, S. L. J. G. b. Ultrafast and memory-
1356 efficient alignment of short DNA sequences to the human genome. **10**, R25 (2009).
1357 77 Anders, S., Pyl, P. T. & Huber, W. J. B. HTSeq—a Python framework to work with
1358 high-throughput sequencing data. **31**, 166-169 (2015).
1359 78 Wang, K., Li, M. & Hakonarson, H. ANNOVAR: functional annotation of genetic
1360 variants from high-throughput sequencing data. *Nucleic acids research* **38**, e164,
1361 doi:10.1093/nar/gkq603 (2010).
1362 79 Subramanian, A. *et al.* Gene set enrichment analysis: a knowledge-based approach for
1363 interpreting genome-wide expression profiles. *Proceedings of the National Academy*
1364 *of Sciences of the United States of America* **102**, 15545-15550,
1365 doi:10.1073/pnas.0506580102 (2005).
1366 80 Quang, D., Chen, Y. & Xie, X. DANN: a deep learning approach for annotating the
1367 pathogenicity of genetic variants. *Bioinformatics* **31**, 761-763,
1368 doi:10.1093/bioinformatics/btu703 (2015).
1369 81 Rentzsch, P., Witten, D., Cooper, G. M., Shendure, J. & Kircher, M. CADD:
1370 predicting the deleteriousness of variants throughout the human genome. *Nucleic*
1371 *acids research* **47**, D886-D894, doi:10.1093/nar/gky1016 (2019).
1372 82 Gulko, B., Hubisz, M. J., Gronau, I. & Siepel, A. A method for calculating
1373 probabilities of fitness consequences for point mutations across the human genome.
1374 *Nature genetics* **47**, 276-283, doi:10.1038/ng.3196 (2015).
1375 83 Li, Q. & Wang, K. InterVar: Clinical Interpretation of Genetic Variants by the 2015
1376 ACMG-AMP Guidelines. *American journal of human genetics* **100**, 267-280,
1377 doi:10.1016/j.ajhg.2017.01.004 (2017).
1378 84 Wu, M. C. *et al.* Rare-variant association testing for sequencing data with the
1379 sequence kernel association test. **89**, 82-93 (2011).
1380 85 Li, B. & Leal, S. M. J. T. A. J. o. H. G. Methods for detecting associations with rare
1381 variants for common diseases: application to analysis of sequence data. **83**, 311-321
1382 (2008).

86 Ionita-Laza, I., Lee, S., Makarov, V., Buxbaum, J. D. & Lin, X. J. T. A. J. o. H. G. Sequence kernel association tests for the combined effect of rare and common variants. **92**, 841-853 (2013).
87 Viechtbauer, W. J. J. o. s. s. Conducting meta-analyses in R with the metafor package. **36**, 1-48 (2010).
88 Becker, B. J. J. T. h. o. r. s. Combining significance levels. 215-230 (1994).
89 M, D. metap: meta-analysis of significance values. *R package version 1.8* (2022).
90 Preston, R. C. *et al.* E-selectin ligand complexes adopt an extended high-affinity conformation. *J Mol Cell Biol* **8**, 62-72, doi:10.1093/jmcb/mjv046 (2016).
91 Qian, J. *et al.* A pan-cancer blueprint of the heterogeneous tumor microenvironment revealed by single-cell profiling. **30**, 745-762 (2020).
92 Zhang, M. *et al.* Dissecting transcriptional heterogeneity in primary gastric adenocarcinoma by single cell RNA sequencing. **70**, 464-475 (2021).
93 McGinnis, C. S., Murrow, L. M. & Gartner, Z. J. J. C. s. DoubletFinder: doublet detection in single-cell RNA sequencing data using artificial nearest neighbors. **8**, 329-337. e324 (2019).
94 Hao, Y. *et al.* Integrated analysis of multimodal single-cell data. **184**, 3573-3587. e3529 (2021).
95 Korsunsky, I. *et al.* Fast, sensitive and accurate integration of single-cell data with Harmony. **16**, 1289-1296 (2019).
96 Wolock, S. L., Lopez, R. & Klein, A. M. J. C. s. Scrublet: computational identification of cell doublets in single-cell transcriptomic data. **8**, 281-291. e289 (2019).
97 Young, M. D. & Behjati, S. J. G. SoupX removes ambient RNA contamination from droplet-based single-cell RNA sequencing data. **9**, giaa151 (2020).
98 Hao, Y. *et al.* Integrated analysis of multimodal single-cell data. *Cell* **184**, 3573-3587 e3529, doi:10.1016/j.cell.2021.04.048 (2021).
99 Patel, A. P. *et al.* Single-cell RNA-seq highlights intratumoral heterogeneity in primary glioblastoma. **344**, 1396-1401 (2014).
100 Yang, J. *et al.* Genetic variance estimation with imputed variants finds negligible missing heritability for human height and body mass index. *Nature genetics* **47**, 1114-1120, doi:10.1038/ng.3390 (2015).
101 Bei, J.-X. *et al.* A GWAS Meta-analysis and Replication Study Identifies a Novel Locus within CLPTM1L/TERT Associated with Nasopharyngeal Carcinoma in Individuals of Chinese AncestryNPC GWAS Follow-up Identifies CLPTM1L/TERT Locus. **25**, 188-192 (2016).
102 Delaneau, O., Marchini, J. & Zagury, J.-F. J. N. m. A linear complexity phasing method for thousands of genomes. **9**, 179-181 (2012).
103 Howie, B. N., Donnelly, P. & Marchini, J. J. P. g. A flexible and accurate genotype imputation method for the next generation of genome-wide association studies. **5**, e1000529 (2009).
104 Luo, C. L. *et al.* RBFOX2/GOLIM4 Splicing Axis Activates Vesicular Transport Pathway to Promote Nasopharyngeal Carcinogenesis. *Adv Sci (Weinh)*, e2004852, doi:10.1002/advs.202004852 (2021).
105 Xu, X. C. *et al.* RNA-binding motif protein RBM47 promotes tumorigenesis in nasopharyngeal carcinoma through multiple pathways. *J Genet Genomics* **48**, 595-605, doi:10.1016/j.jgg.2021.05.006 (2021).

1432 **Figure and table legends**

1433 **Figure 1. Study overview.** A two-stage association study design was applied to investigate the
1434 genetic factors associated with NPC. In the discovery stage, a total of 5,022 samples, including
1435 the GD-SYSUCC cohort from Guangdong in China and the SG cohort from Singapore, were
1436 genotyped with WES and analyzed to identify four independent variants (two of which are
1437 novel), four novel genes, and 59 pathways associated with NPC. The associations were
1438 subsequently validated in the replication stage, which included 9,047 samples from the GD-ZS
1439 cohort in Guangdong and the HK cohort in Hong Kong, China. Bioinformatic analyses and
1440 functional experiments were conducted to explore the biological functions and the clinical
1441 implications of the novel loci.
1442

1443 **Figure 2. Significant pathways and sentinel genes associated with NPC. A**. Significant
1444 pathways associated with NPC. ALLNPC denotes all NPC samples in the discovery stage,
1445 whereas FHNPC represents NPC cases with a familial NPC history. Color bars from white to
1446 purple indicate minus log-transformed P values. **B**. Sentinel genes for NPC-associated
1447 pathways. Genes indicated atop are highlighted in orange if they are part of a specific pathway.
1448 The listed genes are those belonging to at least two NPC-associated pathways and exhibiting a
1449 gene-based association P value below 0.01. **C**. Locations of the rare variants associated with
1450 NPC at significance level of $P < 1\times10^{-4}$ within the genic regions of SELE. Grey arrows denote
1451 non-coding variants, blue arrows represent synonymous coding variants, and the red arrow
1452 indicates non-synonymous coding variant predicted as "deleterious". The rs5361 minor allele
1453 introduces a missense mutation at position 149, resulting in an amino acid substitution from S
1454 to R. The index SNV rs3917410 showed the most significant P value in the association tests in
1455 the discovery stage.
1456

1457 **Figure 3. Expression patterns of novel and known NPC-associated genes across diverse**
1458 **cell types in NPC tumor tissues.** Single-cell transcriptomic analyses of 223,593 cells derived
1459 from NPC tumor tissues in 56 patients. **A**. UMAP plot of 223,593 single cells grouped into
1460 seven major cell clusters. **B**. Violin plot illustrating normalized expression of NPC-associated
1461 genes across these major cell clusters. All epithelial cells captured in NPC tumor were
1462 malignant (see Methods). **C**. The expression of the marker gene (*VWF*) for endothelial cells
1463 and alongside the novel NPC-associated gene *SELE*; top panel: initial UMAP plot, bottom

1464 panel: re-normalized UMAP emphasizing cells highlighted by the red circles in the initial
1465 UMAP plot.
1466

1467 **Figure 4. rs2276868 regulates the expression of RPL14**. **A**. Single-cell transcriptome
1468 analysis showed the mRNA expression of RPL14 in 15,623 malignant epithelial cells from 35
1469 NPC samples with different rs2276868 genotypes. **B**. Relative luciferase activity changes in
1470 293T cells transfected with plasmids containing rs2276868 -[C], -[T], or control vectors. **C**.
1471 Pearson correlation analysis indicates the relationship between *RPL14* and *NKRF* expression
1472 (measured as transcript per million, TPM) in transcriptome data of NPC patients (n=87). **D**.
1473 RT-qPCR illustrates the mRNA expression of RPL14 in NPC cells transfected with NKRF
1474 siRNAs or control siRNA. **E-F**. Relative luciferase activity in 293T cells co-transfected with
1475 the rs2276868 -[C] or -[T] plasmids and NKRF siRNA (F) or NKRF overexpression vectors
1476 (G). Corresponding statistics are presented at the right. **G**. Schematic diagram indicates primer
1477 pairs used for PCR amplification of RPL14 fragments. **H-I**. ChIP assay in S26 cells transfected
1478 with Flag-NKRF and control vectors. ChIP PCR (H) and qPCR (I) showed RPL14 expression
1479 level in cells. P1-3 denote primer pairs targeting genomic regions shown in G. **J**. Pearson
1480 correlation analysis indicates the relationship between NKRF and RPL14 expression in single-
1481 cell transcriptome data are different for NPC patients with different genotypes. rs2276868 -
1482 [CC/CT] patients have a stronger correlation than rs2276868-[TT] patients. *$p < 0.05$, **$p <$
1483 0.01, ***$p < 0.001$.
1484

1485 **Figure 5. *RPL14* inhibits EBV infection and lytic cycle activation in NPC cells. A.** The top
1486 20 pathways significantly associated with RPL14 expression in malignant epithelial cells from
1487 NPC tumor. **B.** Correlation analysis between EBV-activity scores and *RPL14* expression within
1488 malignant epithelial cells. **C.** Single-cell transcriptome analysis showing *LMP1* and *LMP2*
1489 expression in NPC samples with either rs2276868 -[C] or -[T] genotypes. **D.** Western blot
1490 examination of RPL14 and LMP1 protein levels in NPC cell lines S26 and HK-1 cells infected
1491 with EBV at different timepoints. **E**. Western blot assessment of the knockdown efficiency of
1492 RPL14 siRNAs or control siRNA in S26 and HK-1 cells. **F.** Flow cytometry quantification of
1493 GFP intensity for the EBV infection efficiency in the NPC cells described in E. **G**. Western
1494 blot assay showing RPL14 protein expression in S26 and HK-1 cells infected with lentivirus
1495 stably expressing RPL14. ACTIN served as a loading control. **H**. Flow cytometry assessment
1496 of EBV infection efficiency in the cells described in G. **I-J**. Changes of gene expression in

1497 CNE2-EBV cells subjected to EBV lytic induction with TPA and NAB. RT-qPCR (I) and
1498 western blotting (J) were performed to detect the mRNA and protein expression, respectively,
1499 of RPL14 and EBV genes at different timepoints of EBV lytic induction. **K-L**. RT-qPCR
1500 analysis of EBV lytic gene expression in CNE2-EBV and C666-1 cells transfected with RPL14
1501 siRNAs or control siRNA (K), or infected with lentivirus stably expressing RPL14 vector or
1502 control vector (L). *$p < 0.05$, **$p < 0.01$, ***$p < 0.001$, ***$p < 0.0001$.
1503

1504 **Figure 6. Tumor suppressive function of *RPL14* in NPC. A**. Western blot analysis showing
1505 RPL14 protein levels in NPC cells infected with RPL14 overexpressing lentivirus. ACTIN
1506 serves as the loading control. **B**. Cell growth curves of the cells described in A. **C**. Colony
1507 formation assay for the cells described in A. Corresponding statistical analysis is shown to the
1508 right. **D**. Transwell migration assay evaluating the migration ability of the cells described in A.
1509 The statistical analysis is presented on the right. **E-H**. Tumor growth evaluation in a nude mice
1510 model with subcutaneous injection of NPC cells described in A. Tumor volumes were
1511 measured every three days. Visual presentation of tumor post-sacrifice (F) and weight (G) were
1512 presented. IF detection of Ki-67 expression (H) in the tumors described in F, and the
1513 corresponding statistical analysis is shown on the right. **I**. Transcriptomic analysis showcasing
1514 mRNA levels of RPL14 in NPC (n=87) versus control samples (n=10). **J**. Kaplan-Meier
1515 survival analysis linking RPL14 expression to survival time in NPC patients using bulk RNA-
1516 seq data (n=88). *$p < 0.05$, **$p < 0.01$, ***$p < 0.001$, ****$p < 0.0001$.

1517

1518 **Figure 7. SELE-S149R mutation in endothelial cells promotes the tumorigenesis and**
1519 **metastasis of NPC cells. A.** Structure prediction of E-selection paired with glycomimetic
1520 antagonist ligand 2-acetamido-2-deoxy-beta-D-glucopyranose (PDB code 4C16). The spatial
1521 proximity between Ser149 and the ligand is highlighted. Both the Ser149 side chain and the
1522 ligand are shown as sticks, with the distances between the OG atom of Ser149 and the C8 or
1523 O7 atoms of the ligand specified. **B.** Western blot examination of SELE protein level in
1524 HUVEC cells infected with lentivirus overexpressing SELE-WT, S149R mutant or control
1525 vectors. **C.** Transwell migration assay evaluating the migration ability of the cells described in
1526 B, with statistical analysis presented at the bottom. Scale bar, 100 μm. **D.** Tube formation assay
1527 with cells described in B. The statistical analysis is presented on the right. Scale bar, 100 μm.
1528 **E.** Transwell migration assay assessing the migration ability of the NPC cell lines (S26 and
1529 HK-1) co-cultured with HUVEC cells from B (S26/HK-1: HUVEC = 10:1), accompanied by

1530 statistical analysis presented at the bottom. Scale bar, 200 μm. **F-H.** Tumor growth evaluation
1531 in xenograft model with subcutaneous injection of S26 cells described in E. Tumor volumes.
1532 (G) are measured and visual presentation of tumor post-sacrifice (F) and weight (H) are
1533 presented. **I.** IHC staining of CD34 in tumors presented in F. The statistical analysis is
1534 presented on the right. Scale bar, 100 μm. **J-L.** Tumor lymphatic metastasis of S26 cells
1535 described in E. Lymph nodes are visualized (I) and measured (J), with HE staining conducted
1536 to assess metastasis in these lymph nodes (K). Scale bar, 100 μm. *$p < 0.05$, **$p < 0.01$, ***p
1537 < 0.001.
1538

1539 **Figure 8. Contribution of common and rare variants to NPC susceptibility. A**. Fractional
1540 representation of NPC heritability attributable to non-HLA WES-SNVs, categorized by minor
1541 allele frequency (MAF) and linkage disequilibrium (LD). For each variant, MAF was
1542 calculated using the discovery samples, and LD score represented the aggregated R^2 with
1543 adjacent variants spanning a 200kb window. **B**. Density plots illustrating the PRS incorporating
1544 the novel loci and previously known GWAS loci (refined composite PRS, rcPRS) for cases
1545 and controls in both the discovery and replication cohorts. **C**. Receiver operating characteristic
1546 curves comparing the rcPRS and previously reported GWAS PRS (gPRS) for NPC across
1547 different cohorts. **D**. Relative odds ratio comparing the rcPRS or gPRS bins and the 5% lowest
1548 quantile group in different cohorts. **E**. Correlation of rcPRS with disease status in individuals
1549 categorized by their EBV VCA-IgA status.

1550

1551 **Table 1. Association of single variants with NPC susceptibility.** Notes: CHR, chromosome;
1552 A1, effective allele/amino acid; OR (95%CI), odds ratio estimate and the 95% confidence
1553 interval; I^2, the proportion of the variance in observed effect is due to variance in true effects
1554 rather than sampling error; Meta, meta-analyzed using the random effects model.

1555

1556 **Table 2. Associations of individual genes with NPC susceptibility.** Notes: ALLSNV, all
1557 SNVs; SKAT (C+R), SNP-set (Sequence) Kernel Association Test for the combined effect of
1558 common (C) and rare (R) variants; Burden, burden test; Meta, meta-analyzed using the
1559 summation of logits method; Adjusted P, the P value adjusted using the FDR method.
1560